RSC Medicinal Chemistry

ROYAL SOCIETY OF CHEMISTRY

RESEARCH ARTICLE

Published on 01 September 2026
Licensed under CC-BY-NC 4.0

Check for updates

Cite this: *RSC Med. Chem.*, 2026, **17**, 4543

Pyrimidine- and furo[2,3-*d*]pyrimidine-isoxazole hybrids and their Re(I) tricarbonyl complexes with antiproliferative activity against hematological malignancies

Martina Piškor Benković,[a] Ivan Ćorić,[b] Leon Sačer,[a] Lorena Damjanović,[a] Katarina Mišković Špoljarić,[b] Berislav Perić,[c] Srećko I. Kirin,[c] Ljubica Glavaš-Obrovac *[b] and Silvana Raić-Malić *[a]

Pyrimidine and furo[2,3-*d*]pyrimidine derivatives have emerged as promising anticancer agents that act through multiple mechanisms, including modulation of downstream signaling pathways such as a JAK2/STAT3 cascade. Herein, we report the synthesis of novel pyrimidine- and furo[2,3-*d*]pyrimidine-isoxazole hybrids *via* base-promoted 1,3-dipolar cycloaddition and their evaluation for antiproliferative activity. The compounds were assessed *in vitro* against five cancer cell lines (CaCo-2, HeLa, HuT-78, THP-1, and CCRF-CEM) and two non-tumor cell lines (MRC-5 and BJ). Within the 5-alkynyl-substituted pyrimidine series, compound **7g′**, bearing a 5-chloropentynyl substituent, showed the highest activity against the cutaneous T-cell lymphoma HuT-78 (IC_{50} = 20.8 μM). Enhanced antiproliferative activity against HuT-78 cells was observed for the furo[2,3-*d*]pyrimidine isoxazole derivatives **8f′**, **9d′**, and **9f′**, with IC_{50} values of 20.6, 15.5, 16.9 μM, respectively. Coordination to Re(I) improved activity in selected cases: complex $\mathbf{7d'_{Re}}$ showed strong and selective antiproliferative effects against hematological cancer cell lines (IC_{50} = 1.5–2.1 μM, SI > 20), whereas $\mathbf{9f'_{Re}}$ demonstrated notable activity against THP-1 cells (IC_{50} = 2.2 μM, SI > 14). Mechanistic studies in HuT-78 cells revealed that selected derivatives, **8f′**, **9f′**, and **9g′**, induced G0/G1 cell cycle arrest, increasing the G0/G1 population to approximately 57% with a concomitant decrease in the G2/M phase. Collectively, **7g′**, **8f′**, **9d′**, **9f′**, and **9g′** were identify as promising lead compounds with potent antiproliferative activity in HuT-78 cells, mediated through G0/G1 cell-cycle arrest, mitochondrial dysfunction, and modulation of the PI3K/AKT and JAK/STAT signaling pathways. In contrast, the complex $\mathbf{7d_{Re}}$ appears to exert its antiproliferative effects through a cell-cycle-independent mechanism that may involve modulation of the autophagic pathway in HuT-78 cells, without triggering classical apoptosis. These results support the potential of these pyrimidine- and furo[2,3-*d*]pyrimidine-based scaffolds for the development of therapeutic agents targeting T-cell lymphoma and other hematological malignancies.

Received 13th May 2026,
Accepted 27th July 2026

DOI: 10.1039/d6md00379f

rsc.li/medchem

1. Introduction

Hematological malignancies comprise a diverse group of cancers originating from cells of the blood, bone marrow, and lymphatic system, including leukemias, lymphomas, and multiple myeloma.[1,2] Within this group, lymphomas represent a major category of malignancies. Cutaneous T-cell lymphomas (CTCLs) are a distinct subgroup of non-Hodgkin lymphomas that predominantly affect older adults, with an annual incidence of approximately 7.5 cases per million individuals.[3] CTCL progression is driven by interactions between malignant T cells and the skin microenvironment, resulting in disease advancement, immunosuppression, increased susceptibility to infections, and impaired antitumor immune responses. These processes are regulated by several key signaling pathways, including JAK/STAT, MAPK/ERK, PI3K/Akt, and NF-κB. Dysregulation of these pathways is closely associated with CTCL initiation and progression. Consequently, there is a need for small-molecule inhibitors and other targeted therapies capable of addressing the underlying molecular abnormalities in CTCL cells.[4] In this context, nitrogen-containing heterocycles have proven

[a] *Department of Organic Chemistry, University of Zagreb Faculty of Chemical Engineering and Technology, Marulićev trg 20, 10000 Zagreb, Croatia*
[b] *Department of Medicinal Chemistry, Biochemistry and Clinical Chemistry, Faculty of Medicine, Josip Juraj Strossmayer University of Osijek, J. Huttlera 4, 31000 Osijek, Croatia*
[c] *Laboratory for Solid State and Complex Compounds Chemistry, Division of Materials Chemistry, Ruđer Bošković Institute, Bijenička cesta 54, 10000 Zagreb, Croatia*

particularly valuable because of their structural versatility, ability to form hydrogen bonds, and capacity to act as bioisosteres of aromatic π-systems, thereby facilitating efficient interactions with enzymes, receptors, and nucleic acids.[5–9] Among these compounds, pyrimidine derivatives have emerged as privileged scaffolds in anticancer drug design, owing to their favorable pharmacokinetic and pharmacodynamic properties and well-documented antiproliferative activity.[10,11] A prominent example is 5-fluorouracil (5-FU), a widely used pyrimidine-based antimetabolite that remains a cornerstone of cancer therapy despite its known limitations.[12–14] Our previous studies showed that C-5-substituted uracil derivatives exhibited antiproliferative activity against various human cancer cell lines (Fig. 1). Notably, 5-arylethynyl uracil derivative **I** demonstrated activity against HeLa cells,[15] while 5-(furan-2-yl) uracil derivative **II** exhibited greater potency against MCF-7 cells than 5-FU.[16] Additionally, 5-oct-1-ynyl uracil derivative **III** displayed broad cytostatic effects across all tested tumor cell lines.[17] The antiproliferative effect of *N*-methyluracil derivatives was found to be mediated through the suppression of constitutive phosphorylation of STAT3.[18]

The integration of the pyrimidine scaffold with various heterocyclic cores enables the development of hybrid molecules with enhanced biological activity.[19,20] Among these, the furo[2,3-*d*]pyrimidine scaffold, owing to its formal isoelectronic similarity to purine, exhibited a broad range of pharmacological properties, including antiviral and antitumor activity.[21–24] Furo[2,3-*d*]pyrimidine derivatives have been reported to exert anticancer effects through modulation of downstream signaling pathways, including the JAK2/STAT3 cascade, as well as through inhibition of key tyrosine kinases such as c-Met, epidermal growth factor receptor (EGFR), human epidermal growth factor receptor 2 (HER2), and vascular endothelial growth factor receptor 2 (VEGFR-2).[25–29] Furthermore, these scaffolds have been explored as kinase-targeting agents with promising antitumor activity and favorable pharmacokinetic profiles,[30,31] while certain derivatives have also exhibited microtubule depolymerizing activity in different cancer cell models.[32] Our previous studies demonstrated that various 5-substituted and 5,6-disubstituted furo[2,3-*d*]pyrimidine derivatives exhibited pronounced antiproliferative activity against several human cancer cell lines. In particular, the 6-butylfuro[2,3-*d*]pyrimidine derivative **IV** showed significant cytostatic effects against malignant leukemia L1210 cells.[17] Additionally, the furo[2,3-*d*]pyrimidine-1,2,3-triazole hybrid **V**, bearing 5-cyclopropyl and 6-cyclopropylethynyl substituents, displayed marked cytostatic activity against hepatocellular and adenocarcinoma cell lines, surpassing the efficacy of 5-FU (Fig. 1).[33]

Isoxazole-based derivatives have likewise demonstrated significant antitumor potential, particularly through inhibition of the STAT3 signaling pathway, resulting in

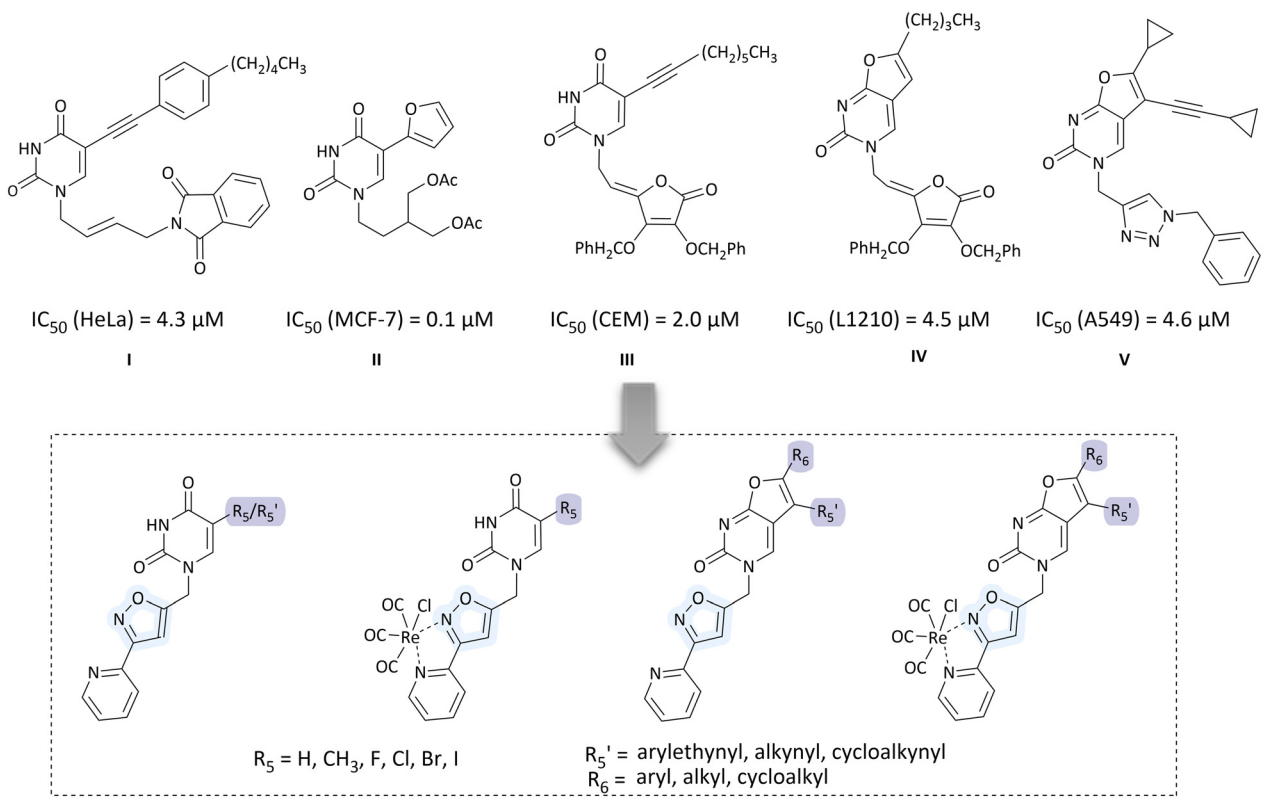

Fig. 1 Design of pyrimidine-**6a**–**6f**, **7a**′–**7e**′, **7g**′, **7h**′ and furo[2,3-*d*]pyrimidine-isoxazole hybrids **8a**′, **8e**′–**8h**′, **9d**′, **9f**′, **9g**′ as well as their Re(I) tricarbonyl complexes $\mathbf{6a_{Re}}$–$\mathbf{6f_{Re}}$, $\mathbf{7d'_{Re}}$, $\mathbf{7g'_{Re}}$ and $\mathbf{9f'_{Re}}$.

 This journal is © The Royal Society of Chemistry 2026

reduced proliferation, induction of apoptosis, and inhibition of cell migration in various cancer models.[34,35]

Furthermore, transition metal complexes have emerged as promising candidates in anticancer drug design, offering improved bioavailability, increased lipophilicity, and redox-mediated biological activity.[36] In particular, rhenium(I) tricarbonyl complexes have shown significant potential and may act through multiple mechanisms, including mitochondrial disruption, enzyme inhibition, DNA interaction, and induction of endoplasmic reticulum stress.[36–38] Notably, these complexes have exhibited stronger *in vitro* antiproliferative activity than cisplatin.[39] Considering the pronounced antiproliferative activity of the aforementioned structural classes, and as an extension of our previous work on pyrimidine,[15–17] furo[2,3-*d*]pyrimidine[17,33] derivatives, as well as isoxazole-based hybrids and Re(I) metal complexes[40–42] with antitumor activity, we have designed and synthesized a series of novel pyrimidine-**6a–6f**, **7a′–7e′**, **7g′**, **7h′** and furo[2,3-*d*]pyrimidine-isoxazole hybrids **8a′**, **8e′–8h′**, **9d′ 9f′**, **9g′** and their Re(I) tricarbonyl complexes $\mathbf{6a_{Re}–6f_{Re}}$, $\mathbf{7d'_{Re}}$, $\mathbf{7g'_{Re}}$ and $\mathbf{9f'_{Re}}$ (Fig. 1). Structural modification at the C-5 position of the pyrimidine scaffold and at the C-5 and C-6 positions of the furo[2,3-*d*]pyrimidine scaffold were introduced to investigate the structure–activity relationship of their antiproliferative activity against various tumor cell lines.

2. Results and discussion

2.1. Synthesis

The synthesis of the targeted pyrimidine-isoxazole hybrids **6a–6f** was carried out through a multistep procedure, as outlined in Scheme 1. Initially, 5-substituted uracil derivatives were subjected to *N*-propargylation using propargyl bromide and sodium hydride, yielding *N*-1-substituted prop-2-ynyl uracil derivatives **2a–2f** as the major products.[43] Subsequent formation of the isoxazole scaffold was efficiently achieved by 1,3-dipolar cycloaddition using a metal-free click approach. The required nitrile oxide was generated *in situ* from the chlorinated aldoxime **5** using triethylamine (Et_3N) as the base.

The resulting nitrile oxide reacted with the corresponding *N*-propargylated uracil derivatives **2a–2f** with high regioselectivity, leading to the formation of 3,5-disubstituted isoxazole regioisomers **6a–6f** in moderate to good yields (17–53%). The pyrimidine-isoxazole hybrids **6a–6f** were subsequently used as bidentate ligands for the preparation of the Re(I) tricarbonyl complexes $\mathbf{6a_{Re}–6f_{Re}}$. These complexes were synthesized by reaction of ligands **6a–6f** with pentacarbonylchlororhenium(I). Due to photosensitivity of Re(I) tricarbonyl complexes, all synthetic and purification steps were carried out under light-protected conditions. To further explore the influence of substituents at the C-5 position of the pyrimidine ring on antiproliferative activity, the study was extended using the Sonogashira cross-coupling reaction to introduce a series of alkynyl groups. Specifically, the 5-iodouracil isoxazole derivative **6f** was reacted with terminal alkynes **a′–h′** in the presence of tetrakis(triphenylphosphine)palladium(0) [$Pd(PPh_3)_4$], copper(I) iodides (CuI), and *N*,*N*-diisopropylethylamine (DIPEA) (Scheme 2). This approach afforded a series of 5-alkynyl uracil isoxazoles **7a′–7e′**, **7g′**, **7h′**. In agreement with our previous findings on 5-alkynyl-substituted uracil derivatives prepared *via* Sonogashira cross-coupling, these reactions yielded not only the expected cross-coupling products but also bicyclic 6-alkylfuro[2,3-*d*]pyrimidines **8a**, **8e′–8h′** and disubstituted 5-alkynyl-6-alkylfuro[2,3-*d*] pyrimidines **9d′**, **9f′**, **9g′** *via* 5-*endo*-dig and 5-*endo*-trig ring closure as shown in Scheme 2.[33] To improve the yields and facilitate the isolation of the 5-alkynyl-substituted pyrimidines **7a′–7e′**, **7g′**, **7h′**, milder reaction conditions were applied during the cross-coupling step. Conversely, selective formation of the cyclic products **8a′**, **8e′–8h′**, **9d′**, **9f′**, **9g′** was achieved by using an excess of alkyne and base at elevated temperatures. In general, the targeted Sonogashira cross-coupling products were successfully synthesized, with the exception of compound **7f′**, which could not be isolated because of rapid intramolecular cyclization leading

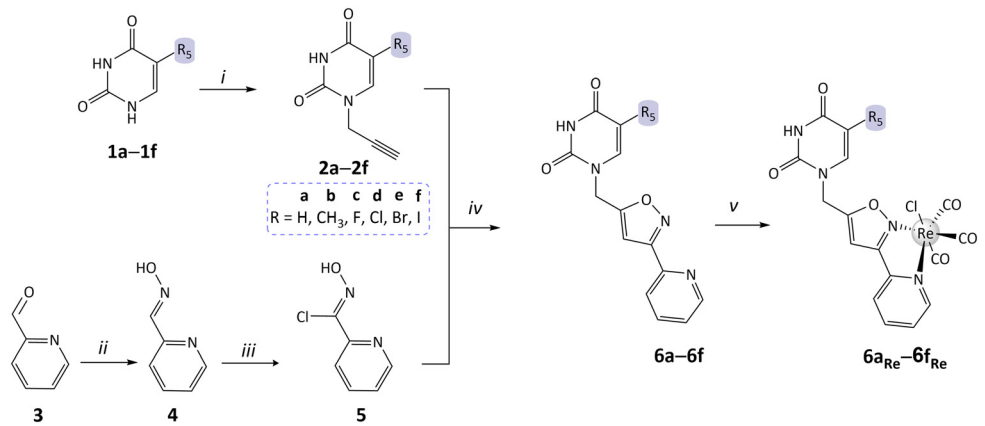

Scheme 1 Reagents and conditions: (i) propargyl bromide, NaH, DMF, rt, 24 h; (ii) $NH_2OH{\cdot}HCl$, CH_3COONa, EtOH, rt, 60 °C, 2 h; (iii) NCS, DMF, 50 °C, 2 h; (iv) CH_2Cl_2, Et_3N, reflux, 24 h; (v) $Re(CO)_5Cl$, $CHCl_3$, reflux, 8 h.

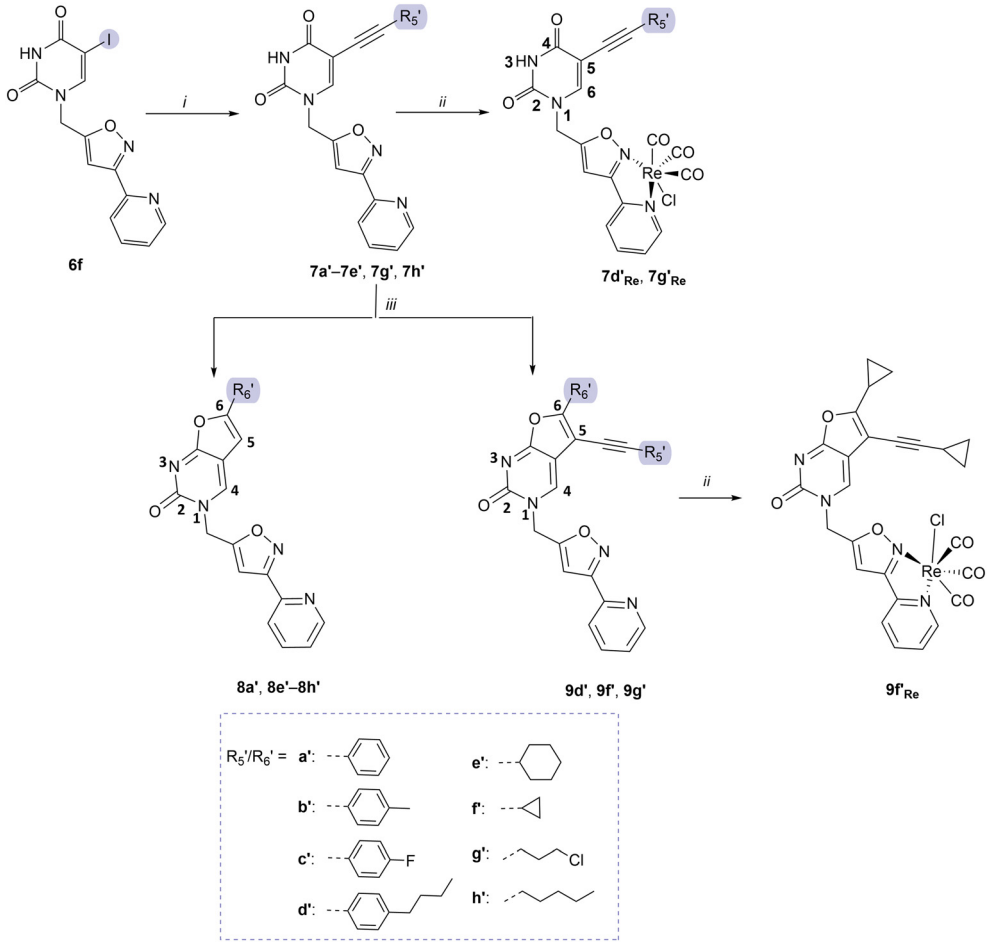

Scheme 2 Reagents and conditions: (i) corresponding terminal alkyne, CuI, $(PPh_3)_4Pd$, *N*,*N*-DIPEA, DMF, r.t., 24 h; (ii) $Re(CO)_5Cl$, $CHCl_3$, reflux, 8 h; (iii) corresponding terminal alkyne, CuI, $(PPh_3)_4Pd$, *N*,*N*-DIPEA, DMF, 80 °C, 48 h.

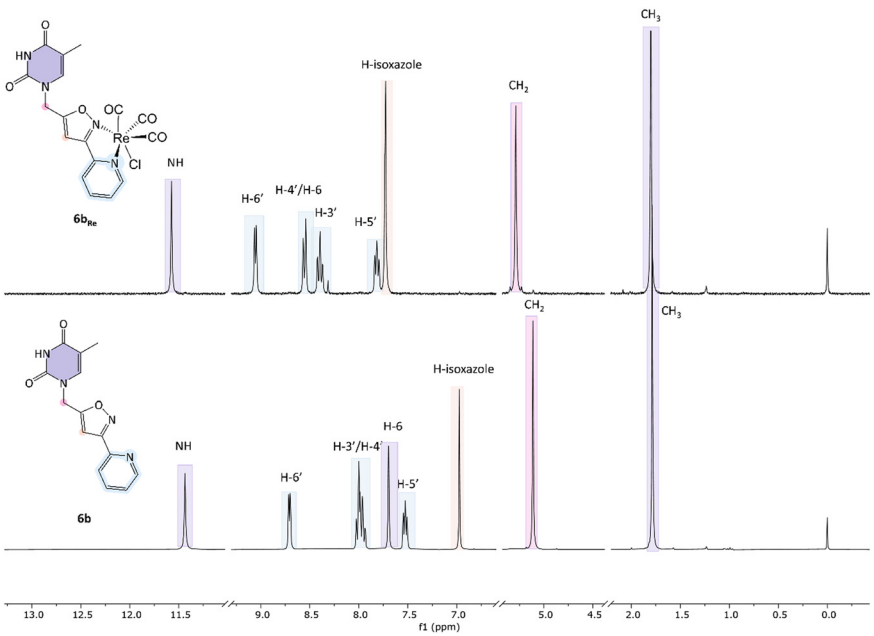

Fig. 2 Comparison of the ^{1}H NMR spectra of ligand **6b** and rhenium(I) tricarbonyl complex $\mathbf{6b_{Re}}$ in DMSO-d_6.

 This journal is © The Royal Society of Chemistry 2026

to furo[2,3-*d*]pyrimidines. Given the relatively low yields of both the 5-alkynyl-substituted pyrimidines and the furo[2,3-*d*]pyrimidines, only compounds exhibiting significant antiproliferative activity (**7d′**, **7g′**, **9f′**) were selected for subsequent complexation. It is noteworthy that rhenium(I) tricarbonyl complexes featuring an octahedral *fac*-Re(CO)$_3$ core are intrinsically chiral when the remaining three coordinative positions are occupied by non-equivalent ligands.[44,45] However, in the absence of a chiral source, all complexes obtained in this study were obtained as racemic mixtures.

2.2. Spectroscopic characterization

The structures of the novel pyrimidine (**6a–6f**, **7a′–7e′**, **7h′**) and furo[2,3-*d*]pyrimidine isoxazoles (**8a′**, **8e′–8h′**, **9d′**, **9f′**, **9g′**) and their Re(I) tricarbonyl complexes (**6a$_{Re}$–6f$_{Re}$**, **7d′$_{Re}$**, **7g′$_{Re}$**, **9f′$_{Re}$**) were determined by analyzing the chemical shifts and H–H coupling constants in the ^{1}H and ^{13}C NMR spectra (Fig. S9 and S38, SI). A notable difference between the ^{1}H NMR spectra of the uncoordinated ligands and their rhenium complexes is the deshielding of the peaks, which is more pronounced for protons closer to the metal atom (Fig. 2).[41,42] This effect is due to the electron-withdrawing influence of Re(I). For example, in the free ligand **6b**, the pyridyl H-6′ signal appears around 8.71 ppm. After coordination to Re(I), the H-6′ signal shifts further downfield to 9.05 ppm, confirming the formation of the metal–N bond. A similar trend is observed for the isoxazole proton, which appears around 6.97 ppm in the free ligand, but shifts downfield to about 7.72 ppm in the complex.

The UV–vis spectra of the complexes in acetonitrile (ACN) show two main features: a high-energy peak between 266 and 275 nm, attributed to an intraligand-π–π* transition, and a lower-energy band between 363 and 377 nm associated with a metal-to-ligand charge transfer (MLCT) transition (Table S3, Fig. S42–S50, SI). To further characterize the synthesized complexes, their stability in aqueous solution and cell culture medium (DMEM, high glucose) was assessed using UV–vis spectroscopy. For this analysis, the pyrimidine complexes **6b$_{Re}$** and **7d′$_{Re}$**, as well as the furo[2,3-*d*]pyrimidine complex **9f′$_{Re}$**, were selected and dissolved in a DMSO/water mixture or cell culture medium. Their spectra were recorded over 24 hours, to monitor possible time-dependent changes in the absorption profiles. Notably, in the 0.01 : 1 (v/v) DMSO–water mixture in the absence of chloride ions, the final spectral trace, marked by a blue shift ($\Delta\lambda_{max} \approx 10$ nm), observed for complexes **6b$_{Re}$** and **9f′$_{Re}$**, was consistent with the formation of the corresponding aqua species through partial aquation (Fig. S51 and S53, SI). This behavior is in agreement with previously reported aquation processes of Re(I) tricarbonyl chloride complexes in aqueous media.[46,47] In cell culture medium, no significant shifts of the absorption maxima of complexes **6b$_{Re}$**, **7d′$_{Re}$** and **9f′$_{Re}$** were observed over 24 h, although a slight decrease in absorption intensity was detected (Fig. S54–S56, SI). This decrease may be attributed to partial aggregation and/or interactions with components of the cell culture medium rather than extensive chemical decomposition.[48,49] To further investigate the stability of the Re(I) tricarbonyl complexes, ^{1}H NMR spectra were recorded immediately after the addition of D_2O to a DMSO-d_6 solution and monitored over 50 h. Upon D_2O addition, the isoxazole proton resonances exhibited a slight upfield shift, indicating a rapid change in the coordination environment. This observation is consistent with partial aquation of the complexes and supports the conclusions drawn from the UV–vis measurements. No additional resonances appeared during the 50 h monitoring period, and all signals remained sharp, indicating that no significant decomposition occurred under the investigated conditions (Fig. S39–S41, SI). The IR spectra (Fig. S57–S74, SI) show three distinct and intense C≡O stretching modes for the symmetric and asymmetric stretching of the carbonyl groups, indicating the *fac*-stereochemistry of the carbonyl groups around the metal center.[40] Two of these modes, in the lower energy range, appear between 1869 and 1949 cm^{-1}, while the third mode is observed between 2018–2036 cm^{-1} (Table S3, SI). The solid-state structures of the pyrimidine ligand **6b**, its rhenium complex **6b$_{Re}$** as methanol solvate and the furo[2,3-*d*]pyrimidine complex **9f′$_{Re}$** were determined by single-crystal X-ray diffraction. Their molecular structures are presented in Fig. 3, full numbering schemes are shown in Fig. S1–S3, packing diagrams are displayed in Fig. S4–S8, while key interatomic distances and angles for the Re(I) complexes summarized in Table S2 (SI). Both complexes **6b$_{Re}$** and **9f′$_{Re}$** adopt the expected octahedral geometry around the d^6-rhenium(I) center, with the three carbonyl ligands arranged in a facial

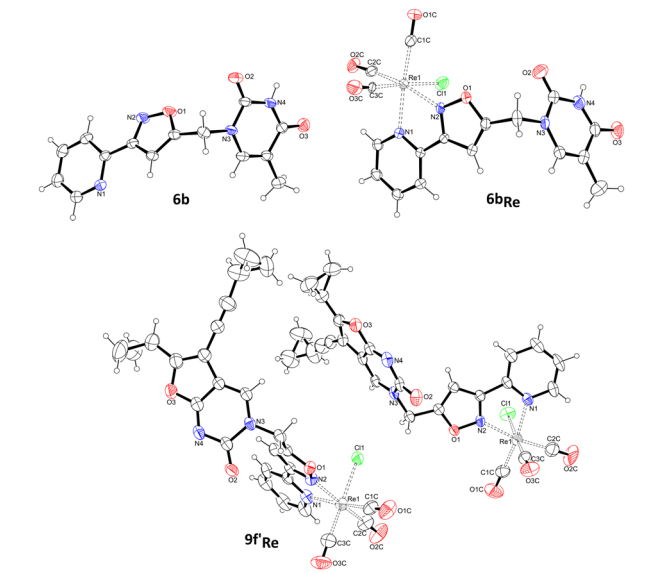

Fig. 3 Crystal structures of the pyrimidine ligand **6b**, its rhenium complex **6b$_{Re}$**, and the furo[2,3-*d*]pyrimidine complex **9f′$_{Re}$**. For **9f′$_{Re}$**, both independent molecules in the unit cell are shown. Only metals, coordinated atoms and heteroatoms are labelled.

configuration, in accordance with IR spectra. The bond lengths and angles observed in these complexes are in good agreement with previously reported structural features of rhenium tricarbonyl complexes with bidentate ligands.[40,46,50]

Table 1 The growth-inhibition effects *in vitro* of pyrimidine-**6a**–**6f**, **7a′**–**7e′**, **7g′**, **7h′** and furo[2,3-*d*]pyrimidine-isoxazole hybrids, **8a′**, **8e′**–**8h′**, **9d′**, **9f′**, **9g′** and their rhenium(I) tricarbonyl complexes $\mathbf{6a_{Re}}$–$\mathbf{6f_{Re}}$, $\mathbf{7d'_{Re}}$, $\mathbf{7g'_{Re}}$, $\mathbf{9f'_{Re}}$ on selected tumor cell lines

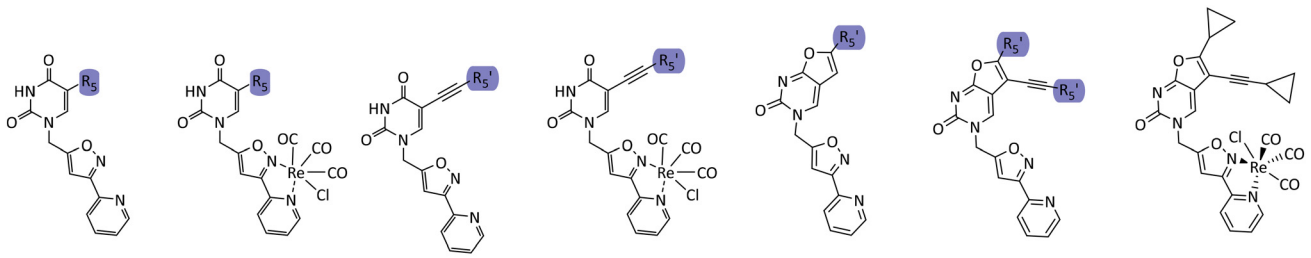

6a–6f **$6a_{Re}$–$6f_{Re}$** **7a′–7e′, 7h′** **$7d'_{Re}$, $7g'_{Re}$** **8a′, 8e′–8h′** **9d′, 9f′, 9g′** **$9f'_{Re}$**

Cpd	R_5/R'_5	IC_{50}[a] (μM) CaCo-2	HeLa	HuT-78	THP-1	CCRF-CEM	BJ	MRC-5	SI[b] (HuT-78)	log $P_{o/w}$[c]
6a	H	>100	>100	92.5 ± 23.5	>100	>100	>100	>100	—	0.12
$6a_{Re}$	H	>100	>100	68.0 ± 11.7	75.2 ± 11.7	69.9 ± 7.8	>100	>100	>1.5	−1.11
6b	CH_3	>100	>100	58.5 ± 15.2	82.9 ± 11.2	>100	>100	>100	>1.7	0.47
$6b_{Re}$	CH_3	>100	>100	67.1 ± 13.9	75.2 ± 2.0	67.8 ± 21.7	>100	>100	>1.5	−0.76
6c	F	>100	>100	53.7 ± 19.4	66.9 ± 10.9	>100	>100	>100	>1.9	0.49
$6c_{Re}$	F	>100	>100	66.5 ± 20.3	65.8 ± 9.4	74.8 ± 16.2	>100	>100	>1.5	−0.74
6d	Cl	>100	>100	60.5 ± 12.9	89.4 ± 19.1	>100	>100	>100	>1.7	0.73
$6d_{Re}$	Cl	>100	>100	71.9 ± 1.2	71.7 ± 9.3	67.4 ± 10.0	>100	>100	>1.4	−0.50
6e	Br	>100	>100	61.1 ± 9.7	65.1 ± 12.5	>100	>100	>100	>1.6	0.81
$6d_{Re}$	Br	>100	>100	83.5 ± 14.6	93.2 ± 7.1	83.1 ± 8.7	>100	>100	>1.2	−0.42
6f	I	>100	>100	82.9 ± 21.7	98.0 ± 23.8	>100	>100	>100	>1.2	0.87
$6f_{Re}$	I	>100	>100	56.8 ± 18.1	66.4 ± 17.9	54.4 ± 12.9	>100	>100	>1.8	−0.37
7a′		>100	>100	71.8 ± 8.7	55.5 ± 13.1	93.9 ± 0.5	>100	>100	>1.4	1.89
7b′		>100	>100	68.5 ± 9.5	64.5 ± 6.2	>100	>100	>100	>1.5	2.24
7c′		>100	>100	>100	71.1 ± 10.0	>100	>100	>100	—	2.25
7d′	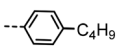	70.5 ± 0.8	>100	42.5 ± 17.3	65.1 ± 1.4	>100	>100	>100	>2.4	3.33
$7d'_{Re}$	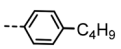	43.0 ± 12.8	38.6 ± 5.7	2.1 ± 0.1	1.6 ± 0.1	1.5 ± 0.6	43.0 ± 12.8	38.6 ± 5.7	20.5	2.08
7e′		>100	>100	55.1 ± 14.6	40.2 ± 3.0	>100	>100	>100	>1.8	2.32
7g′		90.7 ± 1.6	>100	20.8 ± 3.1	29.4 ± 3.4	41.0 ± 16.7	>100	97.6 ± 0.7	>4.8	1.77
$7g'_{Re}$		89.9 ± 16.7	>100	42.7 ± 6.6	24.6 ± 0.2	30.4 ± 5.1	>100	60.1 ± 15.1	>2.3	0.54
7h′	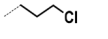	>100	>100	84.8 ± 17.3	90.2 ± 12.2	>100	>100	>100	>1.2	2.34
8a′		>100	>100	86.3 ± 3.9	45.3 ± 2.0	>100	>100	>100	>1.2	1.92
8e′		>100	>100	53.6 ± 11.0	52.8 ± 10.0	>100	>100	>100	>1.8	2.24
8f′		>100	>100	20.6 ± 2.0	45.5 ± 14.5	46.9 ± 20.3	>100	>100	>4.8	1.19
8g′		>100	79.2 ± 2.3	82.9 ± 47.3	23.9 ± 3.3	56.0 ± 8.8	67.9 ± 10.0	>100	0.8	1.78
8h′		>100	68.7 ± 21.4	22.8 ± 0.5	29.4 ± 0.4	43.6 ± 15.3	>100	64.6 ± 11.0	>4.4	2.30
9d′	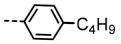	>100	>100	15.5 ± 6.8	37.0 ± 2.4	37.1 ± 9.5 0	>100	87.1 ± 0.3	>6.5	6.37
9f′		98.7 ± 6.6	85.8 ± 19.9	16.9 ± 1.6	42.7 ± 19.5	39.3 ± 9.6	>100	93.1 ± 13.8	>5.9	2.19
$9f'_{Re}$		30.0 ± 1.9	27.6 ± 1.3	27.2 ± 4.0	2.2 ± 7.3	8.9 ± 4.6	31.2 ± 4.2	30.1 ± 3.9	1.1	0.93
9g′		>100	>100	22.2 ± 11.1	>100	90.9 ± 16.7	>100	>100	>4.5	2.97
$Re(CO)_5Cl$		41.6 ± 10.3	>100	>100	>100	33.4 ± 2.3	32.2 ± 0.9	59.5 ± 48.9	—	—
5-FU		5.9 ± 0.7	8.2 ± 1.9	>100	76.4 ± 0.5	52.2 ± 0.8	16.8 ± 7.0	54.1 ± 0.8	—	—
Doxorubicin		5.3 ± 1.1	0.21 ± 0.1	0.03 ± 0.0	0.35 ± 0.1	0.02 ± 0.0	2.15 ± 0.4	0.54 ± 0.1	—	—

[a] 50% inhibitory concentration or compound concentration required to inhibit tumor cell proliferation by 50%, determined after 72 h. [b] Selectivity index, SI = [IC_{50}BJ cells]/[IC_{50}HuT-78 cells]. [c] Calculated lipophilicity values (log *P*) were obtained using the SwissADME online tool (http://www.swissadme.ch/).

This journal is © The Royal Society of Chemistry 2026

As discussed above, **6b$_{Re}$** and **9f′$_{Re}$** are racemic, both complexes crystallise in centrosymmetric point groups $P\bar{1}$ and $P2_1/c$, with both enantiomers present in the unit cell, respectively.

Ligand **6b** and complex **6b$_{Re}$** both contain a pyrimidine H4N–N4 group, where the acidic hydrogen atom is capable of hydrogen bonding. In ligand **6b**, the crystal packing is dominated by hydrogen bonding between the pyrimidine N4–H4N group and the pyridine nitrogen atom N1, connecting the molecules along the *b* crystallographic axis in one-dimensional chain of $\mathbf{C}_1^1(\mathbf{10})$ graph-set notation.[45] In the crystal packing of complex **6b$_{Re}$**, cyclic hydrogen bonded structure with $\mathbf{R}_4^4(\mathbf{12})$ graph set notation are formed,[45] including two molecules of **6b$_{Re}$** and two molecules of the methanol solvent. In addition, aromatic stacking of pyrimidine moieties along the crystallographic *b* axis is found in **6b$_{Re}$**.

2.3. Biological activity

2.3.1. Antiproliferative activity. The novel pyrimidine- (**6a–6f**, **7a′–7e′**, **7g′**, **7h**) and furo[2,3-*d*]pyrimidine-isoxazole (**8a′**, **8e′–8h′**, **9d′**, **9f′**, **9g′**) hybrids and their rhenium(I) tricarbonyl complexes (**6a$_{Re}$–6f$_{Re}$**, **7d′$_{Re}$**, **7g′$_{Re}$**, **9f′$_{Re}$**) were evaluated against five tumor cell lines, with particular emphasis on hematological malignancies, including T-cell lymphoma HuT-78, acute monocytic leukemia THP-1, and acute lymphoblastic leukemia CCRF-CEM, alongside the solid tumor cell lines colon carcinoma CaCo-2 and cervical adenocarcinoma HeLa, as well as two non-tumorigenic human fibroblast cell lines, BJ and MRC-5 (Table 1). The antiproliferative activity of the synthesized compounds was compared with two clinically used anticancer drugs, 5-fluorouracil (5-FU) and doxorubicin (Table 1). Doxorubicin displayed the highest antiproliferative activity toward all tested cancer cell lines, albeit with considerable cytotoxicity toward normal cells. The selectivity indices (SIs) of the ligands and their Re(I) complexes were determined to assess their preferential activity against HuT-78 T-cell lymphoma cells relative to healthy cells. Comparison of pyrimidine isoxazole and furo[2,3-*d*]pyrimidine isoxazole derivatives revealed that the latter scaffold consistently exhibited superior antiproliferative activity across all tested cell lines. This effect was particularly pronounced in lymphoma and leukemia cell lines (HuT-78, THP-1, CCRF-CEM), where these derivatives showed higher efficacy than in colon (CaCo-2) and cervical (HeLa) cancer cells. Although furo[2,3-*d*]pyrimidine derivatives generally showed greater antitumor potency, several C-5-alkynyl-substituted pyrimidines also exhibited significant activity. In particular, compounds **7a′–7e′** and **7g′** showed higher inhibitory activity against HuT-78 and THP-1 cells compared to the unsubstituted **6a**, 5-methyl-**6b** and 5-halogen-substituted **6c–6f** analogs. Among these, the 5-chloropentynyl-substituted pyrimidine **7g′** demonstrated the strongest antiproliferative activity, especially against the HuT-78 cells (IC_{50} = 20.8 μM), with a selectivity index exceeding 4.8. Within the series of 6-substituted furo[2,3-*d*]pyrimidine-isoxazole hybrids, compounds **8f′** and **8h′**, bearing a 6-cyclopropyl and 6-hexyl group, respectively, at the bicyclic core showed the highest cytostatic activity against HuT-78 cells (**8f′**: IC_{50} = 20.6 μM; SI > 4.8; **8h′**: IC_{50} = 22.8 μM; SI > 4.4). Moreover, compound containing 6-(3-chloropropyl) unit exhibited the best inhibitory effect on THP-1 cells (IC_{50} = 23.9 μM). Further comparison between mono- and disubstituted derivatives indicated that 5,6-disubstituted compounds **9f′** and **9g′** exhibited enhanced antiproliferative activity relative to their 6-substituted counterparts **8f′** and **8g′** (Fig. 4). For example, compound **9g′** displayed approximately fourfold higher activity than **8g′** against the HuT-78 cells. Among the 5,6-disubstituted furo[2,3-*d*]pyrimidine derivatives, compounds **9d′** and **9f′** were the most potent. Compound **9d′**, bearing 4-butylphenyl and 1-butyl-4-ethynylphenyl substituent, exhibited the strongest antitumor activity against HuT-78 cells (IC_{50} = 15.5 μM; SI > 6.5). Compound **9f′**, featuring 5-cyclopropyl and 6-cyclopropylethynyl substituents, showed slightly lower activity (IC_{50} = 16.9 μM; SI > 5.9). Antiproliferative evaluation of the Re(I) complexes of the pyrimidine-isoxazole hybrids (**6a$_{Re}$–6f$_{Re}$**) revealed that metal coordination generally led to a modest increase in inhibitory activity against THP-1 and CCRF-CEM cell lines. In contrast, metal coordination of the 5-substituted pyrimidine isoxazole **7d′$_{Re}$** and the 5,6-disubstituted furo[2,3-*d*]pyrimidine **9f′$_{Re}$** complexes resulted in a marked enhancement of antiproliferative activity in both cell lines. In particular, **7d′$_{Re}$** exhibited more than a 40-fold increase in activity against THP-1 and CCRF-CEM cells compared with its corresponding ligand, **7d′**. Notably, selected Re(I) complexes displayed the highest selectivity indices among our previously reported series of Re(I) tricarbonyl complexes, indicating that the present ligand design afforded an improved balance between antiproliferative activity and selectivity.[40–42,51]

Overall, the antiproliferative results revealed several clear structure–activity relationships. As discussed above, conversion of the pyrimidine scaffold into the fused furo[2,3-*d*]pyrimidine system generally enhanced antiproliferative activity, particularly against hematological cancer cell lines. Introduction of C-5 alkynyl substituents and subsequent 5,6-disubstitution further improved activity, with cyclopropyl- and butylphenylethynyl-substituted derivatives being among the most potent. The low calculated log *P* values of compounds **6a–6f** suggest limited lipophilicity, which may contribute to their relatively weak antiproliferative activity. In contrast, alkynyl substitution increased lipophilicity and was generally associated with improved antiproliferative activity. Among the ligands, the 5,6-disubstituted furo[2,3-*d*]pyrimidine derivative **9d′**, which had the highest log *P* value (6.37), also exhibited the greatest antiproliferative activity.

2.3.2. Cell cycle modification. Cell growth and cell cycle progression must be coordinated in order to maintain cell

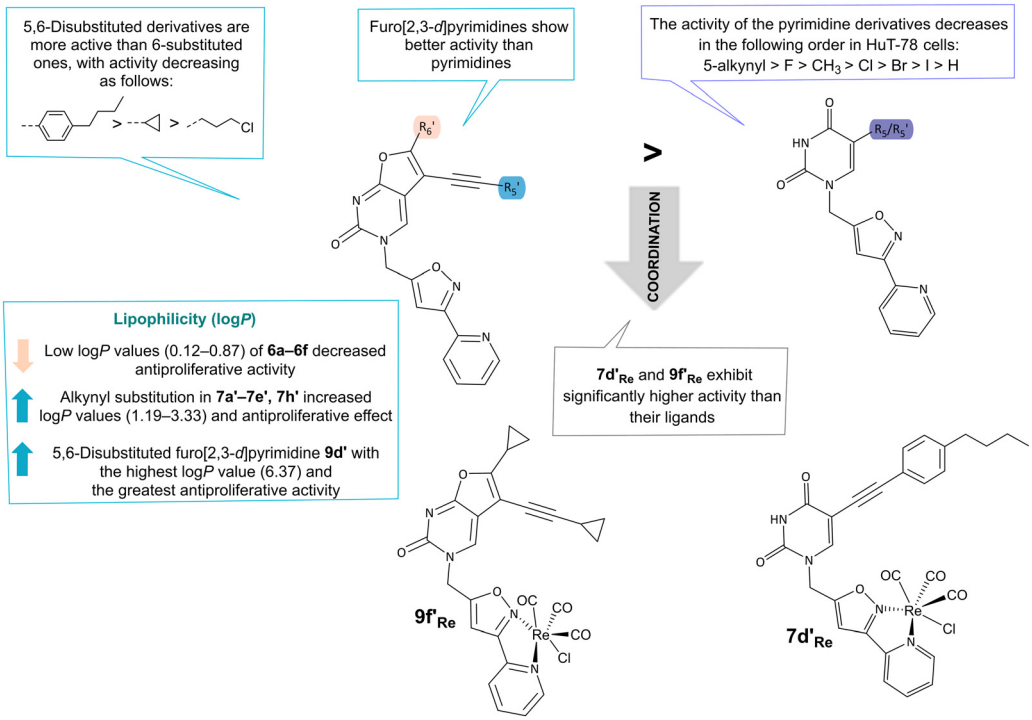

Fig. 4 Insights into the structure–activity relationship in relation to antiproliferative activity for pyrimidine-**6a**–**6f**, **7a**′–**7e**′, **7g**′, **7h**′ and furo[2,3-*d*]pyrimidine-isoxazole hybrids **8a**′, **8e**–**8h**, **9d**′, **9f**′, **9g**′ as well as their Re(I) tricarbonyl complexes $\mathbf{6a_{Re}}$–$\mathbf{6f_{Re}}$, $\mathbf{7d'_{Re}}$, $\mathbf{7g'_{Re}}$ and $\mathbf{9f'_{Re}}$.

viability.[52] Pyrimidine analogs act as anticancer agents through multiple mechanisms, including enzyme inhibition, induction of cell cycle arrest, modulation of oncogene expression, reduction of mitochondrial membrane potential, increase of reactive oxygen species (ROS), and induction of apoptosis in tumor cells.[53] Genetic lesions within the central cell cycle machinery, often leading to its hyperactivation, play a causative role in the development of most tumor types.[54] Accordingly, targeting cell cycle proteins appears to be an effective strategy for inhibiting tumor growth.

Among the tested compounds, the 5-chloropentynyl-substituted pyrimidine **7g**′, the 6-alkyl-substituted furopyrimidine **8f**′, and the 5,6-disubstituted derivatives **9d**′, **9f**′ and **9g**′ showed the most pronounced and selective antiproliferative activity, particularly against HuT-78 cell line compared to non-tumor cells. In addition, the

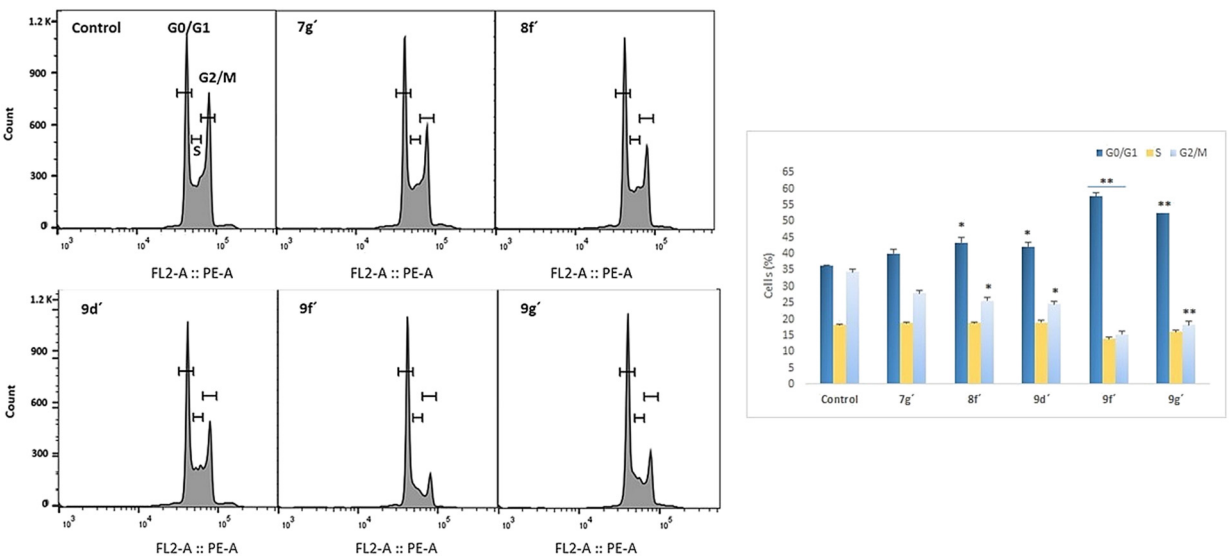

Fig. 5 Flow cytometric analysis of the cell cycle distribution of HuT-78 cells **7g**′, **8f**′, **9d**′, **9f**′, **9g**′ (2×10^{-5} mol L^{-1}) for 24 hours. DNA histograms show changes in the cell cycle. Data are presented as percentage (%) of cells in the cell cycle phase. Statistical significance at confidence level at 95% (Student's *t* – test; $p^* < 0.05$; $p^{**} < 0.01$).

 This journal is © The Royal Society of Chemistry 2026

(4-butylphenyl)ethynyl-substituted pyrimidine isoxazole complex **7d′$_{Re}$** demonstrated notable activity against HuT-78 cells (IC_{50} = 2.1 μM; SI = 20.5). To investigate whether the observed antiproliferative effects of these selected pyrimidine and furopyrimidine derivatives, as well as the pyrimidine isoxazole complex, was associated with disruption of the cell cycle, HuT-78 cells were treated with the selected compounds for 24 h at their respective IC_{50} concentrations. As shown in Fig. 5, the compounds affected cell cycle progression differently. Treatment with the monosubstituted (**8f′**) and disubstituted (**9f′**) furo[2,3-*d*]pyrimidine isoxazoles resulted in a significant accumulation of cells in the G0/G1 phase, increasing from 36.4% in the control group to 43.4% (**8f′**) and 57.6% (**9f′**). Concurrently, the proportion of cells in the G2/M phase decreased markedly (to 25.8% for **8f′** and 15.4% for **9f′**) compared to untreated cells (35.9%). A similar trend was observed for compound **9g′**, which increased the G0/G1 population to 52.6% while reducing the G2/M fraction to 18.3%. The ability of furo[2,3-*d*]pyrimidine and furo[3,2-*e*][1,2,4]triazolo[1,5-*c*]pyrimidine derivatives to arrest cell cycle progression at specific phases was described in the study by Menna *et al.*[26] In addition, a furo[2,3-*d*]pyrimidine-1,3,4-thiadiazole urea derivative was shown to induce pronounced G1-phase arrest (>90%) in K562 myeloid leukemia cells, accompanied by a concentration-dependent increase in the sub-G1 population.[55] In contrast, treatment of HuT-78 cells with the 5-chloropentynyl-substituted compound **7g′** and the (4-butylphenyl)ethynyl-substituted pyrimidine isoxazole complex **7d′$_{Re}$** at their IC_{50} concentrations did not result in significant changes in cell cycle distribution. Obtained results for the 5-chloropentynyl-substituted compound **7g′** could be explain by the fact that pyrimidine-based compounds act *via* multiple pathways designed to halt cancer progression.[56] Given that complex **7d′$_{Re}$** significantly inhibited cell proliferation without inducing detectable cell cycle arrest (Fig. 6a), its mechanism of action may involve alternative cell-cycle independent pathways such as autophagy or other forms of regulated cell death.

2.3.3. Apoptosis and autophagia induction. To further clarify the mechanisms of cell death in HuT-78 cells treated with **7d′$_{Re}$**, its ability to induce apoptosis was investigated. As shown in Fig. 6b, the mechanism of cell death in treated cells is neither apoptosis nor necrosis. Furthermore, because apoptosis, necrosis, and autophagy are the three main modes of tumor cell death[57] and represent the major cellular responses to anticancer therapy, we investigated the ability of **7d′$_{Re}$** to induce the autophagy. Autophagy is a highly conserved lysosome-dependent degradation pathway that maintains cellular homeostasis by recycling damaged organelles and proteins. In cancer, however, autophagy plays a dual role: it may function as a cytoprotective mechanism that promotes tumor cell survival under stress or, alternatively, contribute to autophagic cell death depending on the cellular context and treatment conditions.[58] The autophagy assay revealed statistically significant changes in autophagic activity following treatment with the **7d′$_{Re}$** (Fig. 6c), suggesting that modulation of the autophagic

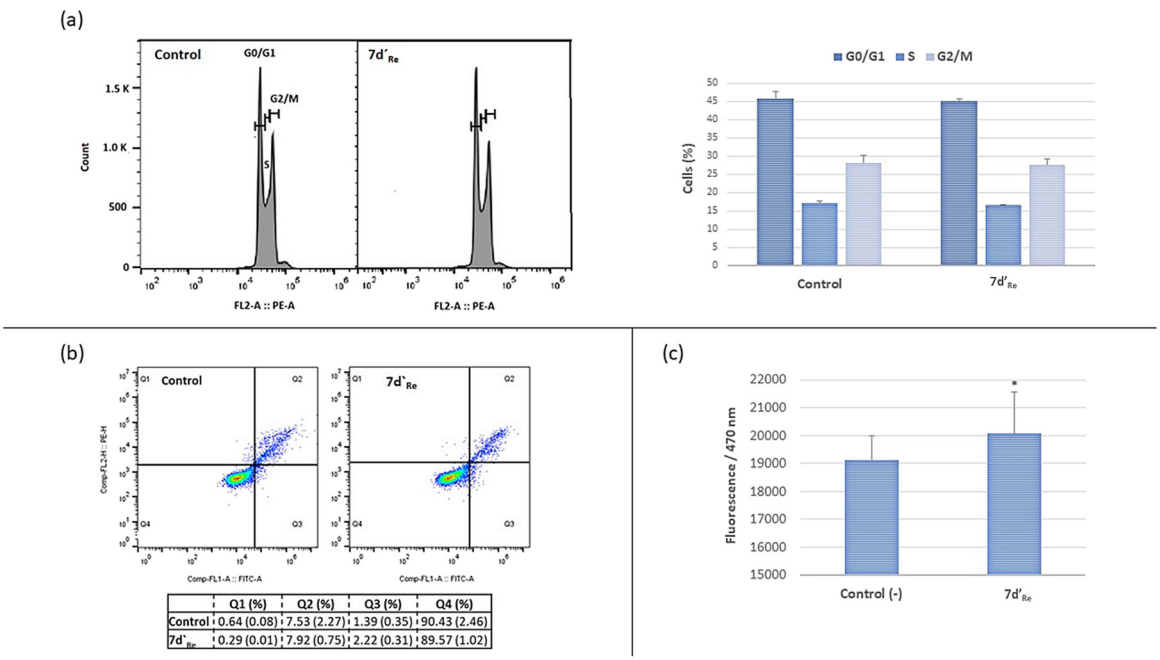

	Q1 (%)	Q2 (%)	Q3 (%)	Q4 (%)
Control	0.64 (0.08)	7.53 (2.27)	1.39 (0.35)	90.43 (2.46)
7d′$_{Re}$	0.29 (0.01)	7.92 (0.75)	2.22 (0.31)	89.57 (1.02)

Fig. 6 Analysis of (a) cell cycle distribution, (b) apoptosis, and (c) autophagy induction in HuT-78 cells exposed to **7d′$_{Re}$** (2×10^{-6} mol L^{-1}) for 24 hours. Cell cycle distribution and apoptosis induction were measured by flow cytometry. Autophagy was determined by fluorescence spectrometry. *statistical significance at the 95% confidence level (Student's *t* – test; $p < 0.05$).

pathway may contribute to its antiproliferative effects without triggering classical apoptosis. However, it is not possible to rule out the possibility that the compound exerts its antiproliferative effect partially through other forms of regulated cell death, such as necroptosis and ferroptosis, as well as through other mechanisms already described for certain rhenium complexes, including the disruption of glutathione metabolism, and endoplasmic reticulum stress.[59]

2.3.4. Total reactive oxygen species (ROS) and superoxide production. ROS are primarily produced in the mitochondria *via* the electron transport chain, where approximately 1–2% of O_2 is reduced to form superoxide anions. Additional sources include peroxisomes, through fatty acid β-oxidation, and the endoplasmic reticulum during protein oxidation.[60] The most biologically relevant ROS involved in both physiological and cancer-related processes are singlet oxygen, superoxide anions, hydroxyl radicals and hydrogen peroxide.[54] To evaluate whether the investigated compounds act as ROS modulators in tumor cells, total ROS and superoxide production were measured in HuT-78 cells following treatment with pyrimidine analog **7g′**, rhenium(I) complex **7d′$_{Re}$**, and the monosubstituted (**8f′**) and disubstituted (**9d′**, **9f′** and **9g′**) furo[2,3-*d*]pyrimidine isoxazole hybrids. These compounds were selected based on their pronounced antiproliferative activity and by analogy with previously reported ROS-modulating agents, including 5-fluorouracil and camphor-based pyrimidine derivatives.[61] As shown in Fig. 7a, only compound **9d′** caused a moderate reduction (approximately 20%) in total intracellular ROS levels compared with untreated HuT-78 cells. Although anticancer agents often increase intracellular ROS levels, the observed decrease suggests that **9d′** may inhibit ROS-generating pathways, which may interfere with cellular processes essential for tumor cell survival. Since superoxide anions are formed during incomplete oxygen redox reactions or ATP synthesis, their production was measured separately. As shown in Fig. 6b, compounds **7g′**, **8f′**, **9d′** and **9f′** decreased the superoxide production by 30%, 24.2%, 19.9%, and 18.7%, respectively. In contrast, compounds **7d′$_{Re}$** and **9g′** produced no significant changes compared with untreated cells (Fig. 7b).

2.3.5. Mitochondrial membrane potential (MMP) analysis. Apoptosis is regulated by two major, interdependent pathways. The extrinsic pathway is triggered by ligand binding to death receptors on the cell surface, whereas the intrinsic apoptotic pathway involves mitochondria and the reduction of mitochondrial membrane potential ($\Delta\Psi_m$), which represent an early event in apoptosis.[62] Recent work by Gorospe and co-workers demonstrated that a decrease in $\Delta\Psi_m$ also serves as an early indicator of mitochondrial stress capable of delaying the G1/S cell cycle transition.[63] Considering these findings and the cell cycle alteration observed following treatment with the investigated compounds at their IC_{50} concentration, we investigated their effects on mitochondrial membrane integrity. As shown in Fig. 7c, compounds **7g′**, **8f′**, and **9d′** at a concentration of 2×10^{-5} mol L^{-1} significantly reduced mitochondrial membrane potential after 24 h of treatment by 46.1%, 53.8% and 22.7%, respectively, compared with untreated HuT-78 cells. In contrast, compounds **9f′** and **9g′** at a concentration of 2×10^{-5} mol L^{-1} exhibited only modest decreases (~15%), while the complex **7d′$_{Re}$** at 2×10^{-6} mol L^{-1} did not significantly affect $\Delta\Psi_m$. Previous studies have demonstrated that pyrimidine-based compounds, can induce cancer cell death through mitochondrial pathways, involving $\Delta\Psi_m$ dissipation, modulation of ROS levels, and activation of apoptosis.[17,21,26] Accordingly, the observed antiproliferative activity of **7g′**, **8f′**, and **9d′** may be associated with activation of the mitochondrial apoptosis pathway.

2.3.6. Effects on protein expression. In cutaneous T-cell lymphoma (CTCL), the PI3K/AKT and JAK/STAT signaling pathways are crucial for cancer cell survival, proliferation, and drug resistance. These pathways are frequently constitutively activated and exhibit extensive crosstalk, thereby reinforcing protumor signaling. Activated STAT3 drives oncogenic genes, while activated AKT promotes survival, and their combined activity. Together with NF-κB, these signaling cascades form an interconnected oncogenic network, making dual targeting a promising therapeutic strategy, particularly in aggressive T-cell lymphomas.[64,65] Western blot and densitometric analyzes were performed to

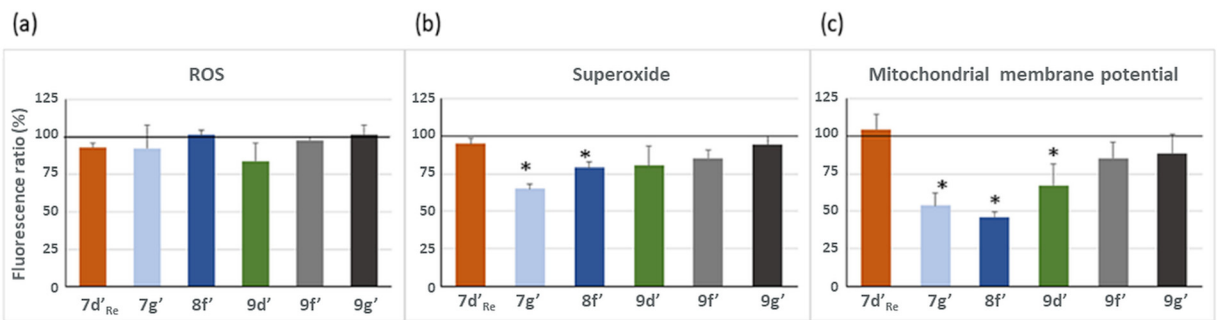

Fig. 7 Evaluation of changes in: a) ROS production; b) superoxide production and c) mitochondrial membrane potential after exposure of HuT-78 cells to **7d′$_{Re}$** (2×10^{-6} mol L^{-1}) and **7g′**, **8f′**, **9d′**, **9f′**, **9g′** (2×10^{-5} mol L^{-1}) for 24 hours. Data are presented as mean and standard deviation of three independent measurements in triplicate. A statistically significant *p* value is defined as $p < 0.05$ (*, #).

 This journal is © The Royal Society of Chemistry 2026

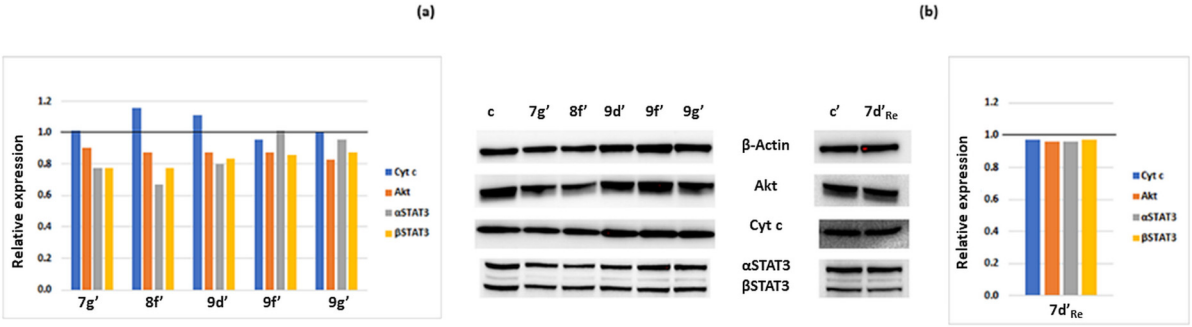

Fig. 8 (a) Western blot analysis of potential cell signaling mediators of antiproliferative effect of compounds $\mathbf{7d'_{Re}}$ (2×10^{-6} mol L^{-1}) and **7g′**, **8f′**, **9d′**, **9f′**, **9g′** (2×10^{-5} mol L^{-1}). Hut-78 cells were cultured in the absence (untreated control) or presence of tested compounds $\mathbf{7d'_{Re}}$ (2×10^{-6} mol L^{-1}) and **7g′**, **8f′**, **9d′**, **9f′**, **9g′** (2×10^{-5} mol L^{-1}) for 24 hours. (b) The expression of selected proteins was measured by densitometry analysis and was normalized to the housekeeping protein β-actin. Results were shown relative to control.

evaluate the effects of the selected compounds on protein expression in the CTCL cell line HuT-78. The expression levels of target proteins were normalized to the housekeeping protein β-actin. As shown in Fig. 8, treatment with compounds **7g′**, **8f′**, **9d′**, **9f′**, and **9g′** at their IC_{50} concentrations altered the expression levels of Akt, STAT3α, and STAT3β. Quantitative analysis revealed a decrease in total Akt expression from 1.0 (control) to 0.9 (**7g′**), 0.82 (**8f′**), 0.88 (**9d′**), 0.85 (**9f′**), and 0.82 (**9g′**). This downregulation may indicate direct inhibition of AKT activity or interference with upstream kinases and pathway crosstalk.[66] STAT3β expression decreased by approximately 20–30% following treatment with all tested compounds, whereas STAT3α expression exhibited compound-dependent variability (Fig. 8a). In HuT-78 cells treated with **7g′**, **8f′**, and **9d′**, STATα levels followed a trend similar to STAT3β, while in cells treated with **9f′** and **9g′**, STAT3α expression remained largely unchanged compared to the control. Constitutive activation of STAT3α plays a pivotal role in the activation of oncogenic pathways, such as cell proliferation, maturation, and survival, while STAT3β is often described as a dominant-negative regulator of cancer. Persistent STAT3 signaling is a well-established oncogenic mechanism in various B-cell lymphomas and the majority of T-cell lymphomas.[67] The observed decrease in STAT3β expression is consistent with previous reports indicating that effective anticancer treatments often reduce STAT3 pathway activity. Notably, modulation of STAT3 isoforms may influence cellular sensitivity to therapy and contribute to apoptotic responses.[68] Western blot analysis of cytochrome C (cyto c) revealed increased levels in cells treated with **8d** and **9f′**, suggesting its release from mitochondria to the cytosol and subsequent activation of cell death pathways.[69] In contrast, treatment with the rhenium(I) complex $\mathbf{7d'_{Re}}$ did not significantly alter the expression levels of Akt, cytochrome c, STAT3α, or STAT3β (Fig. 8b), indicating that this complex likely exerts its antiproliferative effects *via* a mechanism distinct from that of the other tested compounds.

3. Experimental part

3.1. Materials and methods

The reactions were carried out using standard laboratory glassware with chemicals purchased from commercial suppliers and used without further purification. Reaction progress was monitored by thin layer chromatography (TLC) on pre-coated Merck silica gel 60F-254 plates with UV light detection at 254 and 365 nm. For purification, column chromatography was performed with silica gel (Fluka, 0.063–0.2 mm) packed in glass columns prepared by slurrying under gravity. The melting points were determined using a Kofler micro-heating table (Reichert, Vienna). ^{1}H and ^{13}C NMR spectra were recorded with Bruker spectrometers at 300 and 600 MHz, respectively, in DMSO-d_6 at 298 K. The chemical shifts were related to the residual DMSO peak at δ 2.50 ppm for ^{1}H and δ 39.50 ppm for ^{13}C. The assignments of the resonances were based on the chemical shifts, intensities, multiplicities and coupling constants. Elemental analysis was performed using a PerkinElmer 2400 Series II CHNS analyzer, with compositions within 0.4% of theoretical values. Infrared (IR) spectra were recorded using a PerkinElmer Spectrum ONE FT-IR (4000–650 cm^{-1}). The UV/vis absorption spectra of the ligands and rhenium(I) complexes were measured in acetonitrile using a Varian Cary 50 spectrophotometer at 25 °C, covering 200–600 nm with 1 cm quartz cuvettes at 0.1 nm intervals.

Precursors **2a–2f**,[43,70] **4**,[71] and **5** (ref. 72) were prepared following the procedures previously described in the literature.

3.1.1. General procedure for the synthesis of pyrimidine isoxazole derivatives 6a–6f. A stirred solution of the corresponding *N*(1)-propargylated uracil bases **2a–2f** (1 eq.) and pyridine hydroximoyl chloride **5** (1 eq.) in dichloromethane (CH_2Cl_2) was treated with triethylamine (Et_3N) (10 eq.), which was added dropwise. The mixture was then refluxed for 24 hours. After the reaction was complete, the mixture was diluted with dichloromethane (DCM) and washed with water. The combined organic layers were dried

over $MgSO_4$, and the solvent was removed under reduced pressure. The resulting residue was purified by column chromatography (CH_2Cl_2 : MeOH) to yield the desired compounds **6a–6f**.

*1-((3-(Pyridin-2-yl)isoxazol-5-yl)methyl)pyrimidine-2,4(1H,3H)-dione (**6a**).* Compound **6a** was prepared following the general procedure from 1-(prop-2-yn-1-yl)pyrimidine-2,4(1*H*,3*H*)-dione **2a** (150 mg, 0.99 mmol), *N*-hydroxy-2-pyridinecarboximidoyl chloride **5** (156 mg, 0.99 mmol), and triethylamine (1001 mg, 1.4 mL, 9.99 mmol). Product **6a** was isolated as a white powder (108 mg, 39%, m. p. > 250 °C).

^{1}H NMR (300 MHz, DMSO-d_6) δ/ppm: 11.44 (s, 1H, NH), 8.71 (d, J = 4.5 Hz, 1H, H-6′), 7.99 (m, 2H, H-3′, H-4′), 7.82 (d, J = 7.9 Hz, 1H, H-6), 7.52 (ddd, J = 6.9, 4.9, 1.5 Hz, 1H, H-5′), 6.97 (s, 1H, H-isoxazole), 5.67 (d, J = 7.9 Hz, 1H, H-5), 5.15 (s, 2H, CH_2). ^{13}C NMR (75 MHz, DMSO-d_6) δ/ppm: 168.68, 163.59, 162.98, 150.70, 149.98, 147.27, 145.12, 137.57, 125.21, 121.41, 101.90, 101.64, 42.74. IR (ATR) ν/cm^{-1}: 3024, 2801, 1680, 1443, 1404, 1356, 1291, 1228, 1169, 1001, 947, 861, 794, 773. UV (CH_3CN) λ_{max}/nm (ε/dm^3 mol^{-1} cm^{-1}) 261 (20 687). Anal. calcd (%) for $C_{13}H_{10}N_4O_3$ (270.3): C, 57.78; H, 3.73; N, 20.73. Found (%): C, 57.72; H, 3.69; N, 20.81.

*5-Methyl-1-((3-(pyridin-2-yl)isoxazol-5-yl)methyl)pyrimidine-2,4(1H,3H)-dione (**6b**).* Compound **6b** was prepared following the general procedure from 5-methyl-1-(prop-2-yn-1-yl) pyrimidine-2,4(1*H*,3*H*)-dione **2b** (150 mg, 0.91 mmol), *N*-hydroxy-2-pyridinecarboximidoyl chloride **5** (142 mg, 0.91 mmol), and triethylamine (924 mg, 1.3 mL, 9.14 mmol). Product **6b** was isolated as a white powder (115 mg, 44%, m. p. = 219–220 °C).

^{1}H NMR (300 MHz, DMSO-d_6) δ/ppm: 11.43 (s, 1H, NH), 8.71 (d, J = 4.4 Hz, 1H, H-6′), 7.99 (m, 2H, H-6, H-4′), 7.70 (d, J = 1.3 Hz, 1H, H-3′), 7.53 (ddd, J = 7.0, 4.9, 1.5 Hz, 1H, H-5′), 6.97 (s, 1H, H-isoxazole), 5.11 (s, 2H, CH_2), 1.79 (s, 3H, CH_3). ^{13}C NMR (75 MHz, DMSO-d_6) δ/ppm: 168.82, 164.20, 162.96, 150.69, 149.96, 147.28, 140.68, 137.56, 125.20, 121.41, 109.54, 101.67, 42.47, 11.94. IR (ATR) ν/cm^{-1}: 3146, 2953, 2777, 1680, 1460, 1428, 1397, 1373, 1338, 1279, 1217, 1134, 1004, 959, 906, 834, 766, 680. UV (CH_3CN) λ_{max}/nm (ε/dm^3 mol^{-1} cm^{-1}) 267 (8656). Anal. calcd (%) for $C_{14}H_{12}N_5O_3$ (M_r = 284.3): C, 59.15; H, 4.26; N, 19.71. Found (%): C, 59.09; H, 4.22; N, 19.65.

*5-Fluoro-1-((3-(pyridin-2-yl)isoxazol-5-yl)methyl)pyrimidine-2,4(1H,3H)-dione (**6c**).* Compound **6c** was prepared following the general procedure from 5-fluoro-1-(prop-2-yn-1-yl) pyrimidine-2,4(1*H*,3*H*)-dione **2c** (150 mg, 0.89 mmol), *N*-hydroxy-2-pyridinecarboximidoyl chloride **5** (139 mg, 0.89 mmol), and triethylamine (902 mg, 1.2 mL, 8.92 mmol). Product **6c** was isolated as a white powder (53 mg, 21%, m. p. > 250 °C). ^{1}H NMR (600 MHz, DMSO-d_6) δ/ppm: 11.95 (s, 1H, NH), 8.70 (dt, J = 4.9, 1.4 Hz, 1H, H-6′), 8.25 (d, J = 6.6 Hz, 1H, H-6), 8.01 (d, J = 7.8 Hz, 1H, H-3′), 7.96 (td, J = 7.7, 1.7 Hz, 1H, H-4′), 7.52 (ddd, J = 7.4, 4.9, 1.1 Hz, 1H, H-5′), 7.06 (s, 1H, H-isoxazole), 5.09 (s, 2H, CH_2). ^{13}C NMR (151 MHz, DMSO-d_6) δ/ppm: 168.42, 162.98, 157.48 (d, J_{CF} = 25.9 Hz), 149.95, 149.43, 147.30, 140.03 (d, J_{CF} = 230.2 Hz), 137.55, 129.45 (d, J_{CF} = 34.3 Hz), 125.19, 121.42, 101.82, 43.06. IR (ATR) ν/cm^{-1}: 3147, 3030, 2846, 1716, 1691, 1656, 1470, 1420, 1368, 1224, 1140, 959, 909, 842, 785. UV (CH_3CN) λ_{max}/nm (ε/dm^3 mol^{-1} cm^{-1}) 267 (10 820). Anal. calcd (%) for $C_{13}H_9FN_4O_3$ (288.3): C, 54.17; H, 3.15; N, 19.44. Found (%): C, 54.21; H, 3.11; N, 19.35.

*5-Chloro-1-((3-(pyridin-2-yl)isoxazol-5-yl)methyl)pyrimidine-2,4(1H,3H)-dione (**6d**).* Compound **6d** was prepared following the general procedure from 5-chloro-1-(prop-2-yn-1-yl) pyrimidine-2,4(1*H*,3*H*)-dione **2d** (150 mg, 0.81 mmol), *N*-hydroxy-2-pyridinecarboximidoyl chloride **5** (126 mg, 0.81 mmol), and triethylamine (822 mg, 1.1 mL, 8.13 mmol). Product **6d** was isolated as white powder (41 mg, 17%, m. p. > 250 °C). ^{1}H NMR (300 MHz, DMSO-d_6) δ/ppm: 11.97 (s, 1H, NH), 8.71 (d, J = 4.5 Hz, 1H, H-6′), 8.34 (s, 1H, H-6), 8.98 (m, 2H, H-3′, H-4′), 7.52 (m, 1H, H-5′), 7.07 (s, 1H, H-isoxazole), 5.14 (s, 2H, CH_2). ^{13}C NMR (75 MHz, DMSO-d_6) δ/ppm: 168.32, 162.98, 159.45, 149.95, 149.90, 147.29, 142.29, 137.56, 125.19, 121.42, 107.19, 101.87, 43.18. IR (ATR) ν/cm^{-1}: 3148, 2954, 2745, 1691, 1629, 1426, 1399, 1336, 1280, 1225, 1193, 1149, 1061, 962, 911, 791, 767, 660. UV (CH_3CN) λ_{max}/nm (ε/dm^3 mol^{-1} cm^{-1}) 272 (20 286). Anal. calcd (%) for $C_{13}H_9ClN_4O_3$ (304.7): C, 51.25; H, 2.98; N, 18.39. Found (%): C, 51.22; H, 3.07; N, 18.35.

*5-Bromo-1-((3-(pyridin-2-yl)isoxazol-5-yl)methyl)pyrimidine-2,4(1H,3H)-dione (**6e**).* Compound **6e** was prepared following the general procedure from 5-bromo-1-(prop-2-yn-1-yl) pyrimidine-2,4(1*H*,3*H*)-dione **2e** (150 mg, 0.65 mmol), *N*-hydroxy-2-pyridinecarboximidoyl chloride **5** (102 mg, 0.65 mmol) and triethylamine (657 mg, 0.91 mL, 6.51 mmol). Product **6e** was isolated as white powder (43 mg, 19%, m. p. > 250 °C). ^{1}H NMR (300 MHz, DMSO-d_6) δ/ppm: 11.93 (s, 1H, NH), 8.71 (d, J = 4.6 Hz, 1H, H-6′), 8.41 (s, 1H, H-6), 8.10 (m, 2H, H-3′, H-4′), 7.53 (m, 1H, H-5′), 7.06 (s, 1H, H-isoxazole), 5.14 (s, 2H, CH_2). ^{13}C NMR (75 MHz, DMSO-d_6) δ/ppm: 168.35, 162.98, 159.61, 150.11, 149.96, 147.29, 144.66, 137.56, 125.20, 121.42, 101.86, 95.71, 43.14. IR (ATR) ν/cm^{-1}: 3151, 2964, 2768, 1688, 1615, 1420, 1401, 1327, 1222, 1004, 891, 779. UV (CH_3CN) λ_{max}/nm (ε/dm^3 mol^{-1} cm^{-1}) 272 (20 228). Anal. calcd (%) for $C_{13}H_9BrN_4O_3$ (349.1): C, 44.72; H, 2.60; N, 16.05. Found (%): C, 44.79; H, 2.56; N, 16.02.

*5-Iodo-1-((3-(pyridin-2-yl)isoxazol-5-yl)methyl)pyrimidine-2,4(1H,3H)-dione (**6f**).* Compound **6f** was prepared following the general procedure from 5-iodo-1-(prop-2-yn-1-yl) pyrimidine-2,4(1*H*,3*H*)-dione **2f** (150 mg, 0.54 mmol), *N*-hydroxy-2-pyridinecarboximidoyl chloride **5** (85 mg, 0.54 mmol) and triethylamine (550 mg, 0.76 mL, 5.43 mmol). Product **6f** was isolated as white powder (115 mg, 53%, m. p. > 250 °C). ^{1}H NMR (300 MHz, DMSO-d_6) δ/ppm: 11.80 (s, 1H, NH), 8.70 (d, J = 4.6 Hz, 1H, H-6′), 8.39 (s, 1H, H-6), 8.10–7.83 (m, 2H, H-4′, H-3′), 7.53 (m, 1H, H-5′), 7.03 (s, 1H, H-isoxazole), 5.14 (s, 2H, CH_2). ^{13}C NMR (75 MHz, DMSO-d_6) δ/ppm: 168.47, 162.97, 161.01, 150.44, 149.96, 149.22, 147.29, 137.56, 125.20, 121.42, 101.80, 69.38, 42.92. IR (ATR) ν/cm^{-1}: 3122, 3000, 2833, 2028, 1882, 1717, 1670, 1602 1426, 1353, 1290, 1233, 1173, 994, 905, 781, 753. UV

 This journal is © The Royal Society of Chemistry 2026

(CH_3CN) λ_{max}/nm (ε/dm^3 mol^{-1} cm^{-1}) 269 (9547). Anal. calcd (%) for $C_{13}H_9IN_4O_3$ (396.1): C, 39.42; H, 2.29; N, 14.14. Found C, 39.42; H, 2.29; N, 14.14.

3.1.2. General procedure for the synthesis of C-5 alkynyl substituted pyrimidine isoxazoles 7a′–7e′, 7g′, and 7h′ using Sonogashira cross-coupling reaction. To the solution of dry 5-iodo-1-((3-(pyridin-2-yl)isoxazol-5-yl)methyl)pyrimidine-2,4(1*H*,3*H*)-dione **6f** in anhydrous DMF, tetrakis(triphenylphosphine)palladium(0) $(PPh_3)_4Pd$ (0.1 eq.), CuI (0.2 eq) and *N*,*N*-diisopropylethylamine (*N*,*N*-DIPEA) (2.0 eq.) were added under argon atmosphere. The alkyne (1.2 eq.) was then added dropwise and the mixture was stirred at room temperature for 24 hours. After the reaction was complete, the solvent was removed under reduced pressure. The resulting residue was purified by column chromatography to give the desired products **7a′–7e′**, **7g′** and **7h′**.

5-(Phenylethynyl)-1-((3-(pyridin-2-yl)isoxazol-5-yl)methyl)pyrimidine-2,4(1H,3H)-dione (7a′). According to the general procedure, a solution of compound **6f** (150 mg, 0.38 mmol), phenylacetylene (46 mg, 0.05 mL, 0.45 mmol), $Pd(PPh_3)_4$ (44 mg, 0.04 mmol), CuI (14 mg, 0.08 mmol) and DIPEA (98 mg, 1.32 mL, 0.76 mmol) in DMF (3 mL) was stirred under an argon atmosphere. The resulting mixture gave a crude product, which was subsequently purified by column chromatography on silica gel, yielding compound **7a′** as a white solid (15 mg, 11%, m. p. > 250 °C). ^{1}H NMR (300 MHz, DMSO-d_6) δ/ppm: 11.85 (s, 1H, NH), 8.71 (s, 1H, H-6′), 8.40 (s, 1H, H-6), 8.00 (m, 2H, H-3′, H-4′), 7.45 (m, 6H, H-5′, H-2″, H-3″, H-4″), 7.10 (s, 1H, H-isoxazole), 5.19 (s, 2H, CH_2). ^{13}C NMR (151 MHz, DMSO-d_6) δ/ppm: 168.29, 162.98, 161.81, 149.95, 149.72, 148.38, 147.27, 137.55, 131.06, 128.76, 128.68, 125.22, 122.24, 121.45, 101.96, 98.40, 92.04, 81.98, 43.19. Anal. calcd (%) for $C_{21}H_{14}N_4O_3$ (370.4): C, 68.10; H, 3.81; N, 15.13; found (%): C, 68.16; H, 3.77; N, 15.09.

1-((3-(Pyridin-2-yl)isoxazol-5-yl)methyl)-5-(p-tolylethynyl)pyrimidine-2,4(1H,3H)-dione (7b′). According to the general procedure, a solution of compound **6f** (150 mg, 0.38 mmol), 1-ethynyl-4-methylbenzene (53 mg, 0.06 mL, 0.45 mmol), $Pd(PPh_3)_4$ (44 mg, 0.04 mmol), CuI (14 mg, 0.08 mmol) and DIPEA (98 mg, 0.13 mL, 0.76 mmol) in DMF (3 mL) was stirred under an argon atmosphere. The resulting mixture gave a crude product, which was subsequently purified by column chromatography on silica gel, yielding compound **7b′** as a white solid (27 mg, 19%, m. p. > 250 °C). ^{1}H NMR (400 MHz, DMSO-d_6) δ/ppm: 11.82 (s, 1H, NH), 8.68 (m, 1H, H-6′), 8.37 (s, 1H, H-6), 8.01 (m, 2H, H-3′, H-4′), 7.53 (ddd, *J* = 7.4, 4.8, 1.4 Hz, 1H, H-5′), 7.37 (d, *J* = 8.1 Hz, 2H, H-2″), 7.23 (d, *J* = 7.9 Hz, 2H, H-3″), 7.09 (s, 1H, H-isoxazole), 5.19 (s, 2H, CH_2), 2.33 (s, 3H, CH_3). ^{13}C NMR (151 MHz, DMSO-d_6) δ/ppm: 168.29, 162.98, 161.81, 149.95, 149.72, 148.38, 147.27, 137.55, 131.07, 128.76, 128.68, 125.22, 122.24, 121.45, 101.96, 98.40, 92.04, 81.98, 43.20, signal which is assigned to the CH_3 group is obscured by the DMSO signal. Anal. calcd (%) for $C_{22}H_{16}N_4O_3$ (384.4): C, 68.74; H, 4.20; N, 14.58. Found (%): C, 68.69; H, 4.25; N, 14.63.

5-((4-Fluorophenyl)ethynyl)-1-((3-(pyridin-2-yl)isoxazol-5-yl)methyl)pyrimidine-2,4(1H,3H)-dione (7c′). According to the general procedure, a solution of compound **6f** (150 mg, 0.38 mmol), 1-ethynyl-4-fluorobenzene (55 mg, 0.05 mL, 0.45 mmol), $Pd(PPh_3)_4$ (44 mg, 0.04 mmol), CuI (14 mg, 0.08 mmol) and DIPEA (98 mg, 0.13 mL, 0.76 mmol) in DMF (3 mL) was stirred under an argon atmosphere. The resulting mixture gave a crude product, which was subsequently purified by column chromatography on silica gel, yielding compound **7c′** as a white solid (27 mg, 19%, m. p. > 250 °C). ^{1}H NMR (300 MHz, DMSO-d_6) δ/ppm: 11.86 (s, 1H, NH), 8.71 (d, *J* = 4.6 Hz, 1H, H-6′), 8.40 (s, 1H, H-6), 8.99 (m, 2H, H-3′, H-4′), 7.54 (dd, *J* = 7.6, 4.3 Hz, 3H, H–Ph″, H-5′), 7.27 (t, *J* = 8.8 Hz, 2H, H–Ph″), 7.10 (s, 1H, H-isoxazole), 5.20 (s, 2H, CH_2). ^{13}C NMR (75 MHz, DMSO-d_6) δ/ppm: 168.26, 161.93 (d, *J* = 247.6 Hz), 163.28, 161.81, 149.96, 149.71, 148.46, 147.25, 137.57, 133.42 (d, *J* = 8.6 Hz), 125.21, 121.42, 118.68 (d, *J* = 3.3 Hz), 116.04 (d, *J* = 22.1 Hz), 101.95, 98.26, 90.95, 81.69, 54.88, 43.19. Anal. calcd (%) for $C_{21}H_{13}FN_4O_3$ (388.4): C, 64.95; H, 3.37; N, 14.43. Found (%): 65.02; H, 3.43; N, 14.36.

5-((4-Butylphenyl)ethynyl)-1-((3-(pyridin-2-yl)isoxazol-5-yl)methyl)pyrimidine-2,4(1H,3H)-dione (7d′). According to the general procedure, a solution of compound **6f** (150 mg, 0.38 mmol), 1-butyl-4-ethynylbenzene (72 mg, 0.07 mL, 0.45 mmol), $Pd(PPh_3)_4$ (44 mg, 0.04 mmol), CuI (14 mg, 0.08 mmol) and DIPEA (98 mg, 0.13 mL, 0.76 mmol) in DMF (3 mL) was stirred under an argon atmosphere. The resulting mixture gave a crude product, which was subsequently purified by column chromatography on silica gel, yielding compound **7d′** as a white solid (21 mg, 13%, m. p. > 250 °C). ^{1}H NMR (300 MHz, DMSO-d_6) δ/ppm: 11.81 (s, 1H, NH), 8.70 (d, *J* = 4.7 Hz, 1H, H-6′), 8.36 (s, 1H, H-6), 7.96 (m, 2H, H-3′, H-4′), 7.52 (m, 1H, H-5′), 7.37 (d, *J* = 8.0 Hz, 2H, H-2″), 7.23 (d, *J* = 8.1 Hz, 2H, H-3″), 7.08 (s, 1H, H-isoxazole), 5.18 (s, 2H, CH_2), 2.59 (t, *J* = 7.6 Hz, 2H, CH_2″), 1.61–1.46 (m, 2H, CH_2″), 1.29 (m, 2H, CH_2″), 0.88 (t, *J* = 7.3 Hz, 3H, CH_3″). ^{13}C NMR (75 MHz, DMSO-d_6) δ/ppm: 168.31, 163.01, 161.86, 149.97, 149.74, 148.13, 147.30, 143.28, 137.57, 131.03, 128.72, 125.22, 121.44, 119.48, 101.95, 98.60, 92.25, 81.31, 43.18, 34.63, 32.77, 21.68, 13.73. IR (ATR) ν/cm^{-1}: 3046, 2932, 2861, 1693, 1445, 1378, 1346, 1278, 991, 916, 788, 762, 646, 555, 511. UV (CH_3CN) λ_{max}/nm (ε/dm^3 mol^{-1} cm^{-1}) 311 (19 114). Anal. calcd (%) for $C_{25}H_{22}N_4O_3$ (426.5): C, 70.41; H, 5.20; N, 13.14. Found (%): C, 70.49; H, 5.15; N, 13.08.

5-(Cyclohexylethynyl)-1-((3-(pyridin-2-yl)isoxazol-5-yl)methyl)pyrimidine-2,4(1H,3H)-dione (7e′). According to the general procedure, a solution of compound **6f** (150 mg, 0.38 mmol), ethynylcyclohexane (49 mg, 0.06 mL, 0.45 mmol), $Pd(PPh_3)_4$ (44 mg, 0.04 mmol), CuI (14 mg, 0.08 mmol) and DIPEA (98 mg, 0.13 mL, 0.76 mmol) in DMF (3 mL) was stirred under an argon atmosphere. The resulting mixture gave a crude product, which was subsequently purified by column chromatography on silica gel, yielding compound **7e′** as a white solid (17 mg, 12%, m.p. = 210–212 °C). ^{1}H NMR (300 MHz, DMSO-d_6) δ/ppm:

11.67 (s, 1H, NH), 8.71 (d, J = 4.6 Hz, 1H, H-6′), 8.15 (s, 1H, H-6), 7.98 (m, 2H, H-3′, H-4′), 7.53 (m, 1H, H-5′), 7.04 (s, 1H, H-isoxazole), 5.14 (s, 2H, CH_2), 2.63 (m, 2H, H-cyclohexyl), 1.76 (d, J = 9.0 Hz, 2H, H-cyclohexyl), 1.66 (d, J = 5.2 Hz, 2H, H-cyclohexyl), 1.45 (d, J = 11.2 Hz, 2H, H-cyclohexyl), 1.31 (t, J = 7.7 Hz, 3H, H-cyclohexyl). ^{13}C NMR (75 MHz, DMSO-d_6) δ/ppm: 168.40, 162.95, 162.11, 149.95, 149.77, 147.32, 147.28, 137.55, 125.18, 121.41, 101.81, 99.12, 97.17, 72.46, 42.98, 32.09, 28.83, 25.30, 24.14. Anal. calcd (%) for $C_{21}H_{20}ON_4O_3$ (376.4): C, 67.01; H, 5.36; N, 14.88. Found (%): C, 67.06; H, 5.42; N, 14.82.

*5-(5-Chloropent-1-yn-1-yl)-1-((3-(pyridin-2-yl)isoxazol-5-yl)methyl)pyrimidine-2,4(1H,3H)-dione (**7g′**).* According to the general procedure, a solution of compound **6f** (150 mg, 0.38 mmol), 5-chloropent-1-yne (30 mg, 0.05 mL, 0.45 mmol), $Pd(PPh_3)_4$ (44 mg, 0.04 mmol), CuI (14 mg, 0.08 mmol) and DIPEA (98 mg, 0.13 mL, 0.76 mmol) in DMF (3 mL) was stirred under an argon atmosphere. The resulting mixture gave a crude product, which was purified by column chromatography on silica gel, yielding a compound **7g′** as a white solid (28 mg, 22%, m.p. = 186–188 °C). ^{1}H NMR (300 MHz, DMSO-d_6) δ/ppm: 11.70 (s, 1H, NH), 8.71 (d, J = 4.4 Hz, 1H, H-6′), 8.20 (s, 1H, H-6), 8.00 (m, 2H, H-3′, H-4′), 7.52 (m, 1H, H-5′), 7.04 (s, 1H, H-isoxazole), 5.14 (s, 2H, CH_2), 3.76 (t, J = 6.4 Hz, 2H, H-5″), 2.55 (d, J = 6.9 Hz, 2H, H-3″), 1.93 (m, 2H, H-4″). ^{13}C NMR (75 MHz, DMSO-d_6) δ/ppm: 168.36, 162.96, 162.16, 149.96, 149.76, 147.66, 147.27, 137.56, 125.21, 121.43, 101.84, 98.85, 91.77, 73.25, 44.03, 43.05, 30.98, 16.25. IR (ATR) ν/cm^{-1}: 3172, 3042, 1695, 1455, 1374, 1346, 1278, 1219, 993, 917, 854, 789, 762, 656, 547. UV (CH_3CN) λ_{max}/nm (ε/dm^3 mol^{-1} cm^{-1}) 277 (662 338). Anal. calcd (%) for $C_{18}H_{15}ClN_4O_3$ (370.8): C, 58.31; H, 4.08; N, 15.11. Found (%): C, 58.26; H, 4.02; N, 15.16.

*5-(Hept-1-yn-1-yl)-1-((3-(pyridin-2-yl)isoxazol-5-yl)methyl)pyrimidine-2,4(1H,3H)-dione (**7h′**).* According to the general procedure, a solution of compound **6f** (150 mg, 0.38 mmol), hept-1-yne (44 mg, 0.06 mL, 0.45 mmol), $Pd(PPh_3)_4$ (44 mg, 0.04 mmol), CuI (14 mg, 0.08 mmol) and DIPEA (98 mg, 0.13 mL, 0.76 mmol) in DMF (3 mL) was stirred under an argon atmosphere. The resulting mixture gave a crude product, which was purified by column chromatography on silica gel, yielding a compound **7h′** as a white solid (38 mg, 29%, m.p. = 202–204 °C). ^{1}H NMR (300 MHz, DMSO-d_6) δ/ppm: 11.68 (s, 1H, NH), 8.70 (d, J = 4.9 Hz, 1H, H-6′), 8.15 (s, 1H, H-6), 7.98 (d, J = 10.4 Hz, 2H, H-3′, H-4′), 7.52 (t, J = 6.0 Hz, 1H, H-5′), 7.04 (s, 1H, H-isoxazole), 5.14 (s, 2H, CH_2), 2.37 (t, J = 6.5 Hz, 2H, H-3″), 1.48 (m, 2H, H-4″), 1.33 (s, 4H, H-5″, H-6″), 0.87 (t, J = 6.8 Hz, 3H, H-7″). ^{13}C NMR (151 MHz, DMSO-d_6) δ/ppm: 168.38, 162.96, 162.19, 149.95, 149.77, 147.30, 147.27, 137.54, 125.18, 121.41, 101.82, 99.17, 93.52, 72.43, 42.99, 30.41, 27.79, 21.60, 18.67, 13.81. Anal. calcd (%) for $C_{20}H_{20}N_4O_3$ (364.4): C, 65.92; H, 5.53; N, 15.38. Found (%): C, 65.97; H, 5.49; N, 15.47.

3.1.3. General procedure for the synthesis of furo[2,3-*d*]pyrimidine isoxazoles 8a, 8e′–8h′ and 9d′, 9f′, 9g′ using Sonogashira cross-coupling reaction. To the solution of dry 5-iodo-1-((3-(pyridin-2-yl)isoxazol-5-yl)methyl)pyrimidine-2,4(1*H*,3*H*)-dione **6f** in anhydrous DMF, tetrakis(triphenylphosphine)palladium(0) $(PPh_3)_4Pd$ (0.1 eq), CuI (0.3 eq.) and *N*,*N*-diisopropylethylamine (*N*,*N*-DIPEA) (6.0 eq.) were added under argon atmosphere. The alkyne (2.2 eq.) was then added dropwise and the mixture was stirred at 80 °C for 48 hours. After the reaction was complete, the solvent was removed under reduced pressure. The resulting residue was purified by column chromatography to give the desired products **8a**, **8e′**–**8h′** and **9d′**, **9f′** and **9g′**.

*6-Phenyl-3-((3-(pyridin-2-yl)isoxazol-5-yl)methyl)furo[2,3-d]pyrimidin-2(3H)-one (**8a′**).* According to the general procedure, a solution of compound **6f** (150 mg, 0.38 mmol), ethynylbenzene (85 mg, 0.09 mL, 0.83 mmol), $Pd(PPh_3)_4$ (44 mg, 0.04 mmol), CuI (22 mg, 0.11 mmol) and DIPEA (293 mg, 0.39 mL, 2.27 mmol) in DMF (3 mL) was stirred under an argon atmosphere. The resulting mixture gave a crude product, which was purified by column chromatography on silica gel, yielding a compound **8a′** as a white solid (19 mg, 14%, m. p. > 250 °C). ^{1}H NMR (300 MHz, DMSO-d_6) δ/ppm: 11.85 (s, 1H, H-4), 8.71 (d, J = 4.6 Hz, 1H, H-6′), 8.40 (s, 1H, H-5), 7.98 (m, 2H, H–Ar), 7.50 (m, 6H, H–Ar), 7.10 (s, 1H, H-isoxazole), 5.19 (s, 2H, CH_2). ^{13}C NMR (151 MHz, DMSO-d_6) δ/ppm: 171.66, 168.39, 162.94, 154.16, 153.90, 149.90, 147.23, 143.12, 137.50, 129.48, 129.06, 128.18, 125.13, 124.53, 121.34, 107.68, 101.91, 99.31, 46.04. Anal. calcd (%) for $C_{21}H_{14}N_4O_3$ (370.3) C, 68.10; H, 3.81; N, 15.13. Found (%): C, 68.03; H, 3.78; N, 15.17.

*6-(4-butylphenyl)-5-((4-butylphenyl)ethynyl)-3-((3-(pyridin-2-yl)isoxazol-5-yl)methyl]furo[2,3-d]pyrimidin-2(3H)-one (**9d′**).* According to the general procedure, a solution of compound **6f** (150 mg, 0.38 mmol), 1-butyl-4-ethynylbenzene (131 mg, 0.15 mL, 0.83 mmol), $Pd(PPh_3)_4$ (44 mg, 0.04 mmol), CuI (22 mg, 0.11 mmol) and DIPEA (294 mg, 0.39 mL, 2.27 mmol) in DMF (3 mL) was stirred under an argon atmosphere. The resulting mixture gave a crude product, which was purified by column chromatography on silica gel, yielding a compound **9d′** as a white solid (22 mg, 10%, m. p. > 250 °C). ^{1}H NMR (300 MHz, DMSO-d_6) δ/ppm: 9.07 (s, 1H, H-4), 8.68 (d, J = 4.7 Hz, 1H, H-6′), 8.08 (d, J = 8.3 Hz, 2H, H–Ar), 7.96 (d, J = 13.5 Hz, 2H, H–Ar), 7.60 (d, J = 7.8 Hz, 3H, H–Ar), 7.44 (d, J = 8.3 Hz, 2H, H–Ar), 7.32 (d, J = 8.1 Hz, 2H, H-Ar), 7.03 (s, 1H, H-isoxazole), 5.47 (s, 2H, CH_2), 2.65 (d, J = 7.5 Hz, 4H, H-butyl), 1.58 (q, J = 7.5 Hz, 4H, H-butyl), 1.31 (dd, J = 7.2, 4.2 Hz, 4H, H-butyl), 1.22 (s, 1H, H-butyl), 0.90 (m, 5H, H-butyl). ^{13}C NMR (75 MHz, DMSO-d_6) δ/ppm: 170.10, 168.43, 162.99, 154.34, 149.93, 147.29, 145.25, 144.24, 143.23, 137.54, 132.01, 131.97, 131.51, 131.38, 129.22, 128.84, 128.80, 128.64, 125.41, 125.17, 121.38, 118.76, 108.05, 101.86, 98.18, 95.23, 78.23, 34.71, 32.79, 32.71, 21.69, 21.66, 13.71. Anal. calcd (%) for $C_{37}H_{34}N_4O_3$ (582.7): C, 76.27; H, 5.88; N, 9.62. Found (%): C, 76.22; H, 5.83; N, 9.69.

*6-Cyclohexyl-3-((3-(pyridin-2-yl)isoxazol-5-yl)methyl)furo[2,3-d]pyrimidin-2(3H)-one (**8e′**).* According to the general procedure, a solution of compound **6f** (150 mg, 0.38 mmol),

 This journal is © The Royal Society of Chemistry 2026

ethynylcyclohexane (90 mg, 0.09 mL, 0.83 mmol), $Pd(PPh_3)_4$ (44 mg, 0.04 mmol), CuI (22 mg, 0.11 mmol) and DIPEA (294 mg, 0.39 mL, 2.27 mmol) in DMF (3 mL) was stirred under an argon atmosphere. The resulting mixture gave a crude product, purified by column chromatography on silica gel, yielding a compound **8e′** as a white solid (14 mg, 10%, m.p. = 220–222 °C). ^{1}H NMR (300 MHz, DMSO-d_6) δ/ppm: 8.70 (d, J = 4.6 Hz, 1H, H-6′), 8.65 (s, 1H, H-4), 7.98 (t, J = 9.3 Hz, 2H, H-3′, H-4′), 7.52 (t, J = 5.2 Hz, 1H, H-5′), 6.96 (s, 1H, H-isoxazole), 6.45 (s, 1H, H-5), 2.68 (s, 2H, H-cyclohexyl), 1.98 (s, 2H, H-cyclohexyl), 1.77 (s, 3H, H-cyclohexyl), 1.36 (q, J = 13.5, 11.7 Hz, 4H, H-cyclohexyl). ^{13}C NMR (75 MHz, DMSO-d_6) δ/ppm: 168.61, 163.01, 162.64, 154.27, 150.00, 147.30, 141.91, 137.60, 125.23, 121.43, 107.22, 101.87, 45.92, 36.36, 30.03, 25.42, 25.03. Anal. calcd (%) for $C_{21}H_{20}N_4O_3$ (376.4) C, 67.01; H, 5.36; N, 14.88. Found (%): C, 67.06; H, 5.31; N, 14.91.

*6-Cyclopropyl-3-((3-(pyridin-2-yl)isoxazol-5-yl)methyl)furo[2,3-d]pyrimidin-2(3H)-one (**8f′**) and 6-cyclopropyl-5-(cyclopropylethynyl)-3-((3-(pyridin-2-yl)isoxazol-5-yl)methyl)furo-[2,3-d]pyrimidin-2(3H)-one (**9f′**).* According to the general procedure, a solution of compound **6f** (150 mg, 0.38 mmol), ethynylcyclopropane (55 mg, 0.07 mL, 0.83 mmol), $Pd(PPh_3)_4$ (39 mg, 0.04 mmol), CuI (22 mg, 0.11 mmol) and DIPEA (0.39 mL, 2.27 mmol) in DMF (3 mL) was stirred under an argon atmosphere. The resulting mixture gave a crude product, which was purified by column chromatography on silica gel, yielding compound **8f′** (12 mg, 10%, m.p. > 250 °C) and compound **9f′** (28 mg, 19%, m.p. = 214–216 °C), both as white solids. **8f′**: ^{1}H NMR (600 MHz, DMSO-d_6) δ/ppm: 8.69 (s, 1H, H-6′), 8.59 (s, 1H, H-4), 7.99 (d, J = 7.8 Hz, 1H, H-4′), 7.95 (td, J = 7.6, 1.7 Hz, 1H, H-3′), 7.51 (ddd, J = 7.3, 4.8, 1.1 Hz, 1H, H-5′), 6.95 (s, 1H, H-isoxazol), 6.48 (m, 1H, H-5), 5.39 (s, 2H, CH_2), 2.03 (m, 1H, H-cyclopropyl), 0.99 (m, 2H, H-cyclopropyl), 0.88 (m, 2H, H-cyclopropyl). ^{13}C NMR (151 MHz, DMSO-d_6) δ/ppm: 171.55, 168.56, 162.95, 159.62, 154.16, 149.94, 147.26, 140.98, 137.53, 125.18, 121.39, 107.50, 101.83, 97.68, 45.84, 40.04, 8.77, 6.90. Anal. calcd (%) for $C_{18}H_{14}N_4O_3$ (334.1) C, 64.67; H, 4.22; N, 16.76. Found (%): C, 64.72; H, 4.19; N, 16.81. **9f′**: ^{1}H NMR (600 MHz, DMSO-d_6) δ/ppm: 8.73 (s, 1H, H-4), 8.69 (m, 1H, H-6′), 7.97 (m, 2H, H-4′/ H-3′), 7.51 (ddd, J = 7.4, 4.8, 1.3 Hz, 1H, H-5′), 6.95 (s, 1H, H-isoxazole), 5.40 (s, 2H, CH_2), 2.14 (s, 1H, H-cyclopropyl), 1.60 (s, 1H, H-cyclopropyl), 1.12 (m, 2H, H-cyclopropyl), 1.05 (m, 2H, H-cyclopropyl), 0.90 (m, 2H, H-cyclopropyl), 0.79 (m, 2H, H-cyclopropyl). ^{13}C NMR (151 MHz, DMSO-d_6) δ/ppm: 169.90, 168.53, 162.94, 161.41, 154.17, 149.94, 147.29, 141.00, 137.54, 125.17, 121.38, 107.59, 101.74, 100.49, 95.74, 63.33, 46.05, 8.92, 8.61, 7.58. IR (ATR) ν/cm^{-1}: 3088, 3007, 1671, 1650, 1566, 1363, 1175, 1127, 1026, 929, 784, 587. UV (CH_3CN) λ_{max}/nm (ε/dm^3 mol^{-1} cm^{-1}) 210 (24 172). Anal. calcd (%) for $C_{23}H_{18}N_4O_3$ (398.4) C, 69.34; H, 4.55; N, 14.06. Found (%): C, 69.30; H, 4.59; N, 14.11.

*6-(3-Chloropropyl)-3-((3-(pyridin-2-yl)isoxazol-5-yl)methyl)furo[2,3-d]pyrimidin-2(3H)-one (**8g′**) and 5-(5-chloropent-1-yn-1-yl)-6-(3-chloropropyl)-3-((3-(pyridin-2-yl)-isoxazol-5-yl)methyl)furo[2,3-d]pyrimidin-2(3H)-one (**9g′**).* According to the general procedure, a solution of compound **6f** (150 mg, 0.38 mmol), 5-chloropent-1-yne (86 mg, 0.09 mL, 0.83 mmol), $Pd(PPh_3)_4$ (44 mg, 0.04 mmol), CuI (22 mg, 0.11 mmol) and DIPEA (294 mg, 0.39 mL, 2.27 mmol) in DMF (3 mL) was stirred under an argon atmosphere. The resulting mixture gave a crude product, which was purified by column chromatography on silica gel, yielding compound **8g′** (15 mg, 11%, m.p. = 196–198 °C) and compound **9g′** (20 mg, 11%, m.p. = 204–206 °C), both as white solids. **8g′**: ^{1}H NMR (300 MHz, DMSO-d_6) δ/ppm: 8.70 (d, J = 8.5 Hz, 2H, H-4, H-6′), 7.97 (d, J = 9.7 Hz, 2H, H-4′, H-3′), 7.52 (t, J = 5.2 Hz, 1H, H-5′), 6.96 (s, 1H, H-isoxazole), 6.57 (s, 1H, H-5), 5.41 (s, 2H, CH_2), 3.71 (t, J = 6.4 Hz, 2H, H-3″), 2.81 (t, J = 7.1 Hz, 2H, H-2″), 2.09 (m, 2H, H-1″). ^{13}C NMR (151 MHz, DMSO-d_6) δ/ppm: 171.86, 168.52, 162.97, 157.12, 154.20, 149.95, 147.26, 141.90, 137.54, 125.18, 121.37, 107.21, 101.88, 100.23, 54.87, 44.31, 29.33, 24.86. Anal. calcd (%) for $C_{18}H_{15}ClN_4O_3$ (M_r = 370.8) C, 58.31; H, 4.08; N, 15.11. Found (%): C, 58.35; H, 4.03; N, 15.19. **9g′**: ^{1}H NMR (300 MHz, DMSO-d_6) δ/ppm: 8.83 (s, 1H, H-4), 8.69 (d, J = 4.9 Hz, 1H, H-6′), 7.98 (m, 2H, H-4′, H-3′), 7.52 (m, 1H, H-5′), 6.97 (s, 1H, H-isoxazole), 5.43 (s, 2H, CH_2), 3.80 (d, J = 6.4 Hz, 2H, H-5‴), 3.71 (s, 2H, H-3″), 2.92 (t, J = 7.3 Hz, 2H, H-4‴), 2.65 (s, 2H, H-2″), 2.11 (t, J = 6.7 Hz, 2H, H-1″), 2.02 (t, J = 6.6 Hz, 2H, H-3‴). ^{13}C NMR (75 MHz, DMSO-d_6) δ/ppm: 170.48, 168.50, 162.98, 159.79, 154.21, 149.97, 147.29, 142.26, 137.59, 125.22, 121.41, 106.99, 101.83, 98.01, 96.01, 68.89, 46.14, 44.21, 44.14, 30.87, 29.49, 24.00, 16.48. Anal. calcd (%) for $C_{23}H_{20}Cl_2N_4O_3$ (471.3) C, 58.61; H, 4.28; N, 11.89. Found (%): C, 58.57; H, 4.31; N, 11.93.

*6-Pentyl-3-((3-(pyridin-2-yl)isoxazol-5-yl)methyl)furo[2,3-d]pyrimidin-2(3H)-one (**8h′**).* According to the general procedure, a solution of compound **6f** (150 mg, 0.38 mmol), hept-1-yne (80 mg, 0.11 mL, 0.83 mmol), $Pd(PPh_3)_4$ (44 mg, 0.04 mmol), CuI (22 mg, 0.11 mmol) and DIPEA (294 mg, 0.39 mL, 2.27 mmol) in DMF (3 mL) was stirred under an argon atmosphere. The resulting mixture gave a crude product, purified by column chromatography on silica gel, yielding a compound **8h′** (13 mg, 8%, m.p. > 250 °C). ^{1}H NMR (300 MHz, DMSO-d_6) δ/ppm: 8.69 (s, 1H, H-6′), 8.64 (s, 1H, H-4), 7.97 (m, 2H, H-4′, H-3′), 7.52 (m, 1H, H-5′), 6.96 (s, 1H, H-isoxazole), 6.49 (s, 1H, H-7), 5.40 (s, 2H, CH_2), 2.65 (t, J = 7.4 Hz, 2H, H-1″), 1.65 (m, 2H, H-2″), 1.29 (m, 4H, H-3″, H-4″), 0.87 (t, J = 6.9 Hz, 3H, H-5″). ^{13}C NMR (75 MHz, DMSO-d_6) δ/ppm: 171.86, 168.54, 162.98, 158.73, 154.22, 149.95, 147.27, 141.64, 137.54, 125.20, 121.39, 107.28, 101.90, 99.54, 45.86, 30.52, 27.30, 25.97, 21.72, 13.80. Anal. calcd (%) for $C_{20}H_{20}N_4O_3$ (364.4) C, 65.92; H, 5.53; N, 15.38. Found (%): C, 65.96; H, 5.49; N, 15.42.

3.1.4. General procedure for the synthesis of rhenium(I) tricarbonyl complexes ($6a_{Re}$–$6f_{Re}$, $7d'_{Re}$, $7g'_{Re}$, $9f'_{Re}$). Ligands **6a–6f**, **7d′**, **7g′**, **9f′** were dissolved in chloroform, followed by the addition of pentacarbonylchlororhenium(I) $Re(CO)_5Cl$ (1 eq.). The mixture was stirred at reflux temperature in the dark for 8 hours. Upon completion, the mixture was allowed

to cool to room temperature, resulting in the formation of a yellow precipitate of **6a$_{Re}$–6f$_{Re}$**, **7d′$_{Re}$**, **7g′$_{Re}$**, **9f′$_{Re}$**, which was collected by filtration and washed with *n*-hexane.

Complex ***6a$_{Re}$***. Compound **6a$_{Re}$** was synthesized following the general procedure using ligand **6a** (50 mg, 0.18 mmol) and an equimolar amount of $Re(CO)_5Cl$ (67 mg, 0.18 mmol). Product was isolated as a yellow powder through vacuum filtration (45 mg, 42%, m.p. > 250 °C). ^{1}H NMR (300 MHz, DMSO-d_6) δ/ppm: 11.56 (s, 1H, NH), 9.05 (d, J = 5.0 Hz, 1H, H-6′), 8.56 (d, J = 7.8 Hz, 1H, H-6), 8.40 (td, J = 7.9, 1.6 Hz, 1H, H-4′), 7.84 (m, 2H, H-3′, H-5′), 7.74 (s, 1H, H-isoxazole), 5.74 (dd, J = 7.9, 2.1 Hz, 1H, H-5), 5.32 (s, 2H, CH_2). ^{13}C NMR (75 MHz, DMSO-d_6) δ/ppm: 196.95 (CO), 195.81 (CO), 187.70 (CO), 172.67, 164.37, 163.65, 153.99, 150.74, 146.91, 145.00, 140.99, 128.92, 125.92, 102.68, 102.32, 43.45. IR (ATR) ν/cm^{-1}: 3041, 2844, 2018, 1922, 1867, 1697, 1659, 1431, 1373, 1335, 1246, 868, 780. UV (CH_3CN) λ_{max}/nm (ε/dm^3 mol^{-1} cm^{-1}) 258 (23 439); 377 (4501). Anal. calcd (%) for $C_{16}H_{10}ClN_4O_6Re$ (576.9): C, 33.37; H, 1.75; N, 9.73. Found (%): C, 33.39; H, 1.76; N, 9.79.

Complex ***6b$_{Re}$***. Compound **6b$_{Re}$** was synthesized following the general procedure using ligand **6b** (50 mg, 0.18 mmol) and an equimolar amount of $Re(CO)_5Cl$ (64 mg, 0.18 mmol). Product was isolated as a yellow powder through vacuum filtration (51 mg, 49%, m.p. > 250 °C). ^{1}H NMR (300 MHz, DMSO-d_6) δ/ppm: 11.57 (s, 1H, NH), 9.05 (d, J = 5.2 Hz, 1H, H-6′), 8.55 (d, J = 7.7 Hz, 1H, H-4′), 8.39 (td, J = 8.0, 1.4 Hz, 1H, H-3′), 7.83 (ddd, J = 7.3, 5.5, 1.5 Hz, 1H, H-5′), 7.72 (s, 2H, H-6, H-isoxazole), 5.29 (s, 2H, CH_2), 1.80 (s, 3H, CH_3). ^{13}C NMR (75 MHz, DMSO-d_6) δ/ppm: 196.97 (CO), 195.82 (CO), 187.73 (CO), 172.85, 164.38, 164.27, 153.99, 150.75, 146.91, 140.98, 140.61, 128.92, 125.92, 109.84, 102.67, 43.27, 12.03. IR (ATR) ν/cm^{-1}: 3178, 301, 2846, 2036, 1949, 872, 1690, 1441, 1360, 1326, 1226, 986, 953, 781. UV (CH_3CN) λ_{max}/nm (ε/dm^3 mol^{-1} cm^{-1}) 269 (10 327); 375 (2330). Anal. calcd. (%) for $C_{17}H_{12}ClN_4O_6Re$ (589.9): C, 34.61; H, 2.05; N, 9.50. Found (%): C, 34.52; H, 2.11; N, 9.48.

Complex ***6c$_{Re}$***. Compound **6c$_{Re}$** was synthesized following the general procedure using ligand **6c** (50 mg, 0.17 mmol) and an equimolar amount of $Re(CO)_5Cl$ (63 mg, 0.17 mmol). Product was isolated as a yellow powder through vacuum filtration (69 mg, 67%, m.p. > 250 °C). ^{1}H NMR (300 MHz, DMSO-d_6) δ/ppm: 12.11 (d, J = 4.9 Hz, 1H, NH), 9.06 (d, J = 5.1 Hz, 1H, H-6′), 8.50 (d, J = 7.6 Hz, 1H, H-4′), 8.41 (t, J = 7.6 Hz, 1H, H-3′), 8.29 (d, J = 6.6 Hz, 1H, H-6), 7.86 (m, 2H, H-5′, H-isoxazole), 5.27 (s, 2H, CH_2). ^{13}C NMR (75 MHz, DMSO-d_6) δ/ppm: 196.93 (CO), 195.79 (CO), 187.71 (CO), 172.41, 164.35, 157.54 (d, J_{CF} = 25.8 Hz), 154.02, 149.49, 146.87, 141.02, 140.10 (d, J_{CF} = 230.7 Hz), 129.65, 129.19, 128.95, 125.83, 102.82, 43.62. IR (ATR) ν/cm^{-1}: 3073, 3028, 2843, 2018, 1921, 1869, 1707, 1660, 1439, 1375, 1239, 1135, 995, 909, 779. UV (CH_3CN) λ_{max}/nm (ε/dm^3 mol^{-1} cm^{-1}) 269 (17 735); 375 (4002). Anal. calcd (%) for $C_{16}H_9ClFN_4O_6Re$ (593.9): C, 32.36; H, 1.53; N, 9.43. Found (%): C, 32.41; H, 1.50; N, 9.39.

Complex ***6d$_{Re}$***. Compound **6d$_{Re}$** was synthesized following the general procedure using ligand **6d** (50 mg, 0.16 mmol) and an equimolar amount of $Re(CO)_5Cl$ (59 mg, 0.16 mmol). Product was isolated as a yellow powder through vacuum filtration (74 mg, 74%, m.p. = 219–221 °C). ^{1}H NMR (300 MHz, DMSO-d_6) δ/ppm: 12.11 (s, 1H, NH), 9.06 (d, J = 5.1 Hz, 1H, H-6′), 8.50 (d, J = 7.8 Hz, 1H, H-4′), 8.39 (m, 2H, H-3′, H-6), 7.82 (m, 2H, H-5′, H-isoxazole), 5.31 (s, 2H, CH_2). ^{13}C NMR (75 MHz, DMSO-d_6) δ/ppm: 196.92 (CO), 195.82 (CO), 187.75 (CO), 172.30, 164.34, 159.50, 154.02, 149.95, 146.88, 142.24, 141.01, 128.95, 125.85, 107.46, 102.87, 43.74. IR (ATR) ν/cm^{-1}: 3221, 3077, 3000, 2019, 1899, 1701, 1432, 1319, 1225, 1059, 899, 775. UV (CH_3CN) λ_{max}/nm (ε/dm^3 mol^{-1} cm^{-1}) 275 (24 890); 376 (5417). Anal. calcd (%) for $C_{16}H_9Cl_2N_4O_6Re$ (610.4): C, 31.48; H, 1.49; N, 9.18. Found C, 31.52; H, 1.51; N, 9.22.

Complex ***6e$_{Re}$***. Compound **6e$_{Re}$** was synthesized following the general procedure using ligand **6e** (50 mg, 0.14 mmol) and an equimolar amount of $Re(CO)_5Cl$ (51 mg, 0.14 mmol). Product was isolated as a yellow powder through vacuum filtration (82 mg, 87%, m.p. = 234–235 °C). ^{1}H NMR (300 MHz, DMSO-d_6) δ/ppm: 12.08 (s, 1H, NH), 9.06 (d, J = 5.2 Hz, 1H, H-6′), 8.51 (d, J = 7.6 Hz, 1H, H-4′), 8.42 (d, J = 10.5 Hz, 2H, H-3′, H-6), 7.82 (m, 2H, H-5′, H-isoxazole), 5.31 (s, 2H, CH_2). ^{13}C NMR (151 MHz, DMSO-d_6) δ/ppm: 196.92, 195.82, 187.72, 172.31, 164.34, 159.66, 154.00, 150.16, 146.88, 144.58, 141.00, 128.93, 125.86, 102.85, 96.02, 43.71. IR (ATR) ν/cm^{-1}: 3221, 3073, 2024, 1899, 1899, 1656, 1490, 1428, 1323, 1229, 992, 899, 775. UV (CH_3CN) λ_{max}/nm (ε/dm^3 mol^{-1} cm^{-1}) 275 (24 744); 377 (5311). Anal. calcd (%) for $C_{16}H_9BrClN_4O_6Re$ (654.8): C, 29.35; H, 1.39; N, 8.56. Found (%): C, 29.39; H, 1.46; N, 8.50.

Complex ***6f$_{Re}$***. Compound **6e$_{Re}$** was synthesized following the general procedure using ligand **6e** (50 mg, 0.13 mmol) and an equimolar amount of $Re(CO)_5Cl$ (46 mg, 0.13 mmol). Product was isolated as a yellow powder through vacuum filtration (59 mg, 67%, m.p. = 228–230 °C). ^{1}H NMR (600 MHz, DMSO-d_6) δ/ppm: 11.93 (s, 1H, NH), 9.05 (m, 1H, H-6′), 8.52 (m, 1H, H-4′), 8.42 (s, 1H, H-6), 8.40 (td, J = 7.8, 1.5 Hz, 1H, H-3′), 7.82 (ddd, J = 7.8, 5.4, 1.4 Hz, 1H, H-5′), 7.76 (s, 1H, H-isoxazole), 5.31 (dd, J = 5.2, 1.0 Hz, 2H, CH_2). ^{13}C NMR (151 MHz, DMSO-d_6) 196.91, 195.81, 187.70, 172.44, 164.33, 161.06, 153.98, 150.49, 149.12, 146.89, 140.98, 128.91, 125.87, 102.77, 79.14, 69.81, 43.53. IR (ATR) ν/cm^{-1}: 3159, 2968, 1724, 1685, 1603, 1412, 1354, 1221, 1004, 903. UV (CH_3CN) λ_{max}/nm (ε/dm^3 mol^{-1} cm^{-1}) 266 (24758); 375 (4885). Anal. calcd (%) for $C_{16}H_9BrIN_4O_6Re$ (M_r = 701.8): C, 27.38; H, 1.29; N, 7.98. Found (%): C, 27.42; H, 1.25; N, 8.00.

Complex ***7d′$_{Re}$***. Compound **7d′$_{Re}$** was synthesized following the general procedure using ligand **7d′** (50 mg, 0.12 mmol) and an equimolar amount of $Re(CO)_5Cl$ (42 mg, 0.12 mmol). Product was isolated as a yellow powder through vacuum filtration (45 mg, 52%, m.p. > 250 °C). ^{1}H NMR (600 MHz, DMSO-d_6) δ 11.96 (s, 1H, NH), 9.07 (dt, J = 5.4, 1.2 Hz, 1H,

This journal is © The Royal Society of Chemistry 2026

H-6′), 8.53 (dt, J = 7.9, 1.1 Hz, 1H, H-4′), 8.41 (td, J = 7.8, 1.5 Hz, 1H, H-3′), 8.39 (s, 1H, H-6), 7.83 (m, 2H, H-5′, H-isoxazole), 7.38 (m, 2H, H-2″), 7.24 (m, 2H, H-3″), 5.38 (m, 2H, CH_2), 2.60 (t, J = 7.7 Hz, 2H, CH_2″), 1.56 (m, 2H, CH_2″), 1.30 (m, J = 7.4 Hz, 2H, CH_2″), 0.90 (t, J = 7.4 Hz, 3H, CH_3″). ^{13}C NMR (151 MHz, DMSO) δ 197.42 (CO), 196.34 (CO), 188.23 (CO), 172.80, 164.86, 162.41, 154.51, 150.28, 148.53, 147.40, 143.86, 141.52, 131.54, 129.45, 129.24, 126.37, 119.88, 103.43, 99.45, 92.93, 81.66, 44.29, 35.14, 33.28, 22.18, 14.23. IR (ATR) ν/cm^{-1}: 3079, 2933, 2025, 1931, 1898, 1703, 1674, 1464, 1372, 1239, 789, 620, 530. UV (CH_3CN) λ_{max}/nm (ε/dm^3 mol^{-1} cm^{-1}) 308 (23 603); 377 (7473). Anal. calcd (%) for $C_{28}H_{22}ClN_4O_6Re$ (732): C, 45.93; H, 3.03; N, 7.65. Found (%): C, 45.97; H, 3.28; N, 7.61.

Complex **7g′$_{Re}$**. Compound **7g′$_{Re}$** was synthesized following the general procedure using ligand **7g′** (50 mg, 0.13 mmol) and an equimolar amount of $Re(CO)_5Cl$ (49 mg, 0.13 mmol). Product was isolated as a yellow powder through vacuum filtration (20 mg, 22%, m.p. = 209–210 °C). ^{1}H NMR (600 MHz, DMSO-d_6) δ 11.85 (s, 1H, NH), 9.06 (ddd, J = 5.4, 1.5, 0.8 Hz, 1H, H-6′), 8.52 (ddd, J = 7.9, 1.4, 0.8 Hz, 1H, H-4′), 8.41 (td, J = 7.8, 1.5 Hz, 1H, H-3′), 8.23 (s, 1H, H-6), 7.83 (ddd, J = 7.8, 5.4, 1.4 Hz, 1H, H-5′), 7.78 (s, 1H, H-isoxazole), 5.37–5.27 (m, 2H, CH_2), 3.77 (t, J = 6.4 Hz, 2H, CH_2″), 2.55 (t, J = 6.9 Hz, 2H, CH_2″), 1.95 (p, J = 6.7 Hz, 2H, CH_2″). ^{13}C NMR (151 MHz, DMSO-d_6) δ 197.42 (CO), 196.33 (CO), 188.21 (CO), 172.86, 164.85, 162.72, 154.50, 148.08, 147.39, 141.51, 129.44, 126.38, 103.33, 99.71, 92.51, 73.70, 44.51, 44.18, 31.47, 16.74. IR (ATR) ν/cm^{-1}: 3080, 2919, 2848, 2030, 1914, 1875, 1696, 1438, 1333, 1239, 993, 969, 783, 643, 623, 531. UV (CH_3CN) λ_{max}/nm (ε/dm^3 mol^{-1} cm^{-1}) 290 (822 511); 377 (3804). Anal. calcd (%) for $C_{21}H_{15}Cl_2N_4O_6Re$ (676.5): C, 45.93; H, 3.03; N, 7.65. Found (%): C, 45.90; H, 3.06; N, 7.68.

Complex **9f′$_{Re}$**. Compound **9f′$_{Re}$** was synthesized following the general procedure using ligand **9f′** (50 mg, 0.13 mmol) and an equimolar amount of $Re(CO)_5Cl$ (45 mg, 0.13 mmol). Product was isolated as a yellow powder through vacuum filtration (45 mg, 51%, m.p. > 250 °C). ^{1}H NMR (600 MHz, DMSO-d_6) δ 9.06 (dt, J = 5.3, 1.2 Hz, 1H, H-6′), 8.78 (s, 1H, H-4), 8.49 (dt, J = 7.9, 1.1 Hz, 1H, H-4′), 8.39 (td, J = 7.8, 1.5 Hz, 1H, H-3′), 7.82 (ddd, J = 7.8, 5.4, 1.4 Hz, 1H, H-5′), 7.66 (s, 1H, H-isoxazole), 5.60–5.52 (m, 2H, CH_2), 2.17 (tt, J = 8.4, 5.1 Hz, 1H, H-cyclopropyl), 1.61 (tt, J = 8.2, 5.0 Hz, 1H, H-cyclopropyl), 1.16–1.12 (m, 2H, H-cyclopropyl), 1.09–1.05 (m, 2H, H-cyclopropyl), 0.97–0.92 (m, 2H, H-cyclopropyl), 0.82–0.77 (m, 2H, H-cyclopropyl). ^{13}C NMR (151 MHz, DMSO) δ 197.41 (CO), 196.34 (CO), 188.22 (CO), 172.88, 170.55, 170.40, 164.83, 162.10, 154.71, 154.49, 147.38, 141.62, 141.50, 129.42, 126.32, 108.34, 103.49, 101.22, 96.31, 96.30, 63.65, 46.95, 40.42, 40.28, 40.14, 40.00, 39.86, 39.72, 39.58, 9.46, 9.13, 8.16, 0.42. IR (ATR) ν/cm^{-1}: 3071, 3004, 2030, 1936, 1916, 1903, 1680, 1572, 1560, 1429, 1366, 1203, 924, 790, 531. UV (CH_3CN) λ_{max}/nm (ε/dm^3 mol^{-1} cm^{-1}) 210 (42 597); 363 (7935). Anal. Calcd for: $C_{26}H_{18}ClN_4O_6Re$ (704) C, 44.35; H, 2.58; N, 7.96. Found (%): C, 44.38; H, 2.54; N, 7.99.

3.2. Evaluation of the antiproliferative activity

3.2.1. Cell lines and cell cultivation. The effect of the newly synthesized compounds was tested on human tumor cell lines, including T lymphoblasts (acute lymphoblastic leukemia) CCRF-CEM, monocytes (acute monocytic leukemia) THP1, cervical adenocarcinoma HeLa, colon adenocarcinoma CaCo-2, T-cell lymphoma HuT-78 and non-tumorous human fibroblast cell lines BJ and MRC-5. Cells were cultured in two different types of media: DMEM and RPMI 1640. Both medias were supplemented with 2 mM glutamine, fetal bovine serum (10% heat inactivated) and antibiotics (100 U penicillin and 0.1 mg streptomycin). The RPMI 1640 was additionally enriched with 10 mM HEPES and 1 mM sodium pyruvate. The cells growing in a monolayer were cultured in DMEM, while the cells growing in suspension were cultured in RPMI 1640. The cells were grown in a CO_2 incubator (IGO 150 CELLlifeTM, JOUAN) at 37 °C in a humidified atmosphere with 5% CO_2.

3.2.2. Proliferation assay. Growth inhibitory activity was assessed using a slightly modified procedure based on the National Cancer Institute protocol.[73] In brief, cells were seeded in 96-well microtiter plates and incubated for 24 hours and then treated with 10^{-7} to 10^{-4} M concentrations of the tested compounds for an additional 72 hours. After the treatment period, the effects of the tested compounds on the growth rate of the cells were examined using the MTT assay.[74] The absorbance was measured at 595 nm using a microplate reader. The IC_{50} values, representing 50% inhibition of cell growth, and the QC calculation were performed using GraphPadPrism and Excel software. The effect of each concentration was analyzed by plotting the logarithm of the concentration of the tested substance against the corresponding percentage inhibition value using least squares.

3.2.3. Cell cycle analysis. HuT-78 cells were plated in 24-well plates at a concentration of 1 × 10^5 cells per well and treated with the exposed to **7d$_{Re}$** (2 × 10^{-6} mol L^{-1}) and **7g′**, **8f′**, **9d′**, **9f′**, **9g′** (2 × 10^{-5} mol L^{-1}) for 24 hours. After treatment with the compounds, the cells were fixed with ice-cold 70% ethanol in phosphate-buffered saline (PBS) and incubated with 0.3 μg mL^{-1} propidium iodide for 30 minutes at room temperature. Prior to analysis by flow cytometry (BD FACSLyric, Becton Dickinson, San Jose, CA, USA), samples were treated with 0.4 μg mL^{-1} RNase A for 5 minutes at room temperature. The resulting DNA histograms were generated and analyzed using FlowJo 10.10. software (Treestar, Inc., Ashland, OR, USA).

3.2.4. Determination of apoptosis. Cell apoptosis was assessed using the Annexin V-FITC/PI Apoptosis Kit (Elabscience, E-CK-A211, Wuhan, China) according to the manufacturer's instructions. Briefly, cells were seeded in

6-well plates and then treated with the tested compound for 24 hours. After treatment, the cells were collected, washed with PBS, and centrifuged at 300 × *g* for 5 minutes. After removing the supernatant, the cells were washed again with PBS and resuspended in 500 μL of 1× annexin V binding buffer, after which 5 μL of annexin V-FITC and 5 μL of PI reagent were added. The samples were incubated for 20 minutes in the dark to allow specific binding of the reagents to the cells. After incubation, the samples were analyzed using a flow cytometer (BD FACSLyric, Becton Dickinson, San Jose, CA, USA). Based on the Annexin V-FITC signal, viable and necrotic cells were distinguished from early and late apoptotic cells. Doxorubicin was used as a positive control.

3.2.5. Determination of autophagy. Autophagy activity in cells was determined using a commercial autophagy detection kit (Autophagy Detection Kit; Abcam, ab139484, Cambridge, United Kingdom). After treatment with the tested compound, the cells were washed with 1× assay buffer. For cell staining, a solution of Green Detection Reagent and Hoechst 33342 with 5% FBS was prepared. A total of 100 μL of dye was added to each well, and the cells were incubated for 30 minutes at 37 °C in the dark. To remove excess dye, the cells were then washed twice with 1× assay buffer, and 100 μL of buffer was added to each well. For the measurement, a multimodal microtiter plate reader (Tecan Spark, Tecan, Switzerland) was used. Fluorescence of the Green Detection Reagent was measured with an excitation wavelength of approximately 480 nm and an emission wavelength of approximately 530 nm. Simultaneously, fluorescence of Hoechst 33342 was measured with an excitation wavelength of 340 nm and an emission wavelength of 480 nm. Rapamycin was used as a positive control. Chloroquine is included in the kit as an inhibitor control, and the combination of rapamycin and chloroquine was used to monitor autophagic flux.

3.2.6. Measurement of the mitochondrial membrane potential ($\Delta\Psi_m$). In a black wall/clear bottom 96-well plate, 5 × 10^5 cells were seeded and incubated with compounds **7d′$_{Re}$** (2 × 10^{-6} mol L^{-1}) and **7g′**, **8f′**, **9d′**, **9f′**, **9g′** (2 × 10^{-5} mol L^{-1}) for 24 hours at 37 °C (5% CO_2). Treatment was removed and rhodamine 123 (Sigma-Aldrich, St. Louis, MO, USA) was added to a final concentration of 5 μM. Following a 30 min incubation at 37 °C (5% CO_2), the dye was removed, cells were washed with PBS, resuspended in PBS and analyzed using Tecan Spark (Tecan, Männedorf, Switzerland) microplate reader with fluorescence filter settings (Ex/Em = 485/530 nm) and the Sparkcontrol Method Editor software. Results are expressed as values relative to control. Each compound was tested in a triplicate.

3.2.7. Determination of intracellular free oxygen radicals (ROS) and superoxide production. HuT-78 cells were resuspended at a concentration of 1 × 10^5 cells per mL in PBS and incubated for 1 hour in an incubator at 37 °C/5% CO_2 with **7d′$_{Re}$** (2 × 10^{-6} mol L^{-1}) and **7g′**, **8f′**, **9d′**, **9f′**, and **9g′** (2 × 10^{-5} mol L^{-1}). At the end of the incubation period, reagents were added to the cells according to the manufacturer's instructions from the Fluorometric Intracellular Ros Kit (Sigma-Aldrich, St. Louis, USA) and the cells were then incubated in an incubator at 37 °C/5% CO_2 for 30 minutes. Cell analysis was performed with Tecan Spark Multimode Microplate Reader (Tecan, Mannedorf, Switzerland) using the Sparkcontrol Method Editor software. Intracellular free oxygen radicals are detected with a green fluorescence filter setting (Ex/Em = 490/595 nm), while superoxide production was detected by an orange fluorescence signal (Ex/Em = 550/620 nm). Experiments were performed in triplicate and quantitative data are expressed as mean ± standard deviation. STATISTICA 14.0.1.8. (TIBCO Software Inc., Tulsa, USA) was used to statistically analyze the results. Student's *t*-test was used to analyze the data. A *p*-value of less than 0.05 was considered statistically significant.

3.2.8. Western blot analysis. For protein expression analysis, cells were treated for 24 h with the following compounds **7d′$_{Re}$** (2 × 10^{-6} mol L^{-1}) and **7g′**, **8f′**, **9d′**, **9f′** and **9g′** (2 × 10^{-5} mol L^{-1}). Treated cells were lysed using a lysis buffer containing 50 mM Tris (pH 7.5), 150 mM NaCl, 2 mM Na_2EDTA, 1% SDS, and cOmplete™ Mini, EDTA-free protease inhibitor (Roche Diagnostics, Indianapolis, IN, USA). Samples were mixed with mPAGE™ 4× LDS Sample Buffer (Merck, Darmstadt, Germany), separated using mPAGE™ MOPS SDS Running Buffer (Merck, Darmstadt, Germany), and transferred with mPAGE™ Transfer Buffer (Merck, Darmstadt, Germany). Antibodies GAPDH Rabbit mAb (Cell Signaling, Danvers, MA, USA), Cytochrome c Rabbit mAb (Cell Signaling, Danvers, MA, USA), Akt (pan) mAb (Cell Signaling, Danvers, MA, USA), STAT3 Rabbit pAb (Merck, Darmstadt, Germany), and Goat pAb to Rb IgG (HRP) (Abcam, Cambridge, UK) were prepared according to a slightly modified manufacturer's protocol. Detection was performed using Immobilon™ Western Chemiluminescent HRP Substrate (Merck, Darmstadt, Germany) and ChemiDoc™ Imaging System (Bio-Rad Laboratories, Hercules, CA, USA). Protein expressions were analyzed by densitometric analysis using Fiji ImageJ 1.54p software,[75] results were normalized to β-actin and presented as relative values compared to the control.

3.3. X-ray crystallography

The X-ray intensity data for **6b**, **6b$_{Re}$** and **9f′$_{Re}$** were collected on XtaLAB Synergy (Dualflex) CCD diffractometer using monochromatic Cu-Kα (λ = 1.54184 Å) radiation at room temperature. The basic experimental data are given in Table S1 in SI. The data were processed with the CrysAlisPro program,[76] which was used for the determination of unit cells and data reduction. The structures were solved by direct methods using the program SHELXT[77] and refined against F^2 on all data by a full-matrix least squares procedure with the program SHELXL.[78] All non-hydrogen atoms are refined in the anisotropic atomic displacement parameter (ADP) model.

 This journal is © The Royal Society of Chemistry 2026

In the **6b$_{Re}$** structure, the refined C3CA–O3CA bond length of 0.994(7) Å in one of the coordinated carbonyl groups indicates a possible disorder with Cl^- anions coordinated on the other side of the Re atom. This type of disorder is similar with related structures in the literature,[41] but incorporating this disorder into the **6b$_{Re}$** structure model only slightly improves the final *R* value and several additional restraints need to be introduced to keep the refinement stable. Therefore, the final structural model of **6b$_{Re}$** was refined without this type of disorder. The positions of hydrogen atoms were treated in the riding model, *i.e.* they were calculated according to the positions of the carbon atoms to which they are bonded. C–H distances for aromatic, methylene and methyl H-atoms were constrained to 0.93, 0.97 and 0.96 Å, respectively, with isotropic ADP parameter $U_{iso}(H) = 1.2 \times U_{iso}(C)$ for aromatic and methylene H-atoms and $U_{iso}(H) = 1.5 \times U_{iso}(C)$ for methyl H-atoms. Torsion angles of the methyl groups were refined. The CCDC 2551645–2551647 contain the supplementary crystallographic data for this paper.

4. Conclusions

A series of novel pyrimidine- and furo[2,3-*d*]pyrimidine isoxazoles, along with selected *fac*-Re(I) tricarbonyl complexes, was successfully synthesized and structurally characterized using ^{1}H NMR, ^{13}C NMR, IR, and UV–vis spectroscopy, as well as single-crystal X-ray diffraction for representative compounds. The employed synthetic strategy enabled efficient synthesis of structurally diverse derivatives, while Sonogashira cross-coupling of the 5-iodopyrimidine precursor afforded both 5-alkynyl-substituted pyrimidines and fused furo[2,3-*d*]pyrimidine derivatives *via* intramolecular 5-*endo*-dig and 5-*endo*-trig cyclization. Biological evaluation revealed a structure–activity relationship, indicating that fused furo[2,3-*d*]pyrimidine derivatives generally exhibit superior antiproliferative activity compared to their pyrimidine counterparts, particularly against hematological cancer cell lines. Among the synthesized compounds, derivatives **7g′**, **8f′**, **9d′**, **9f′**, and **9g′** showed the most promising activity, with **9d′** and **9f′** showing the most favorable activity/selectivity profiles in HuT-78 cells. Rhenium coordination did not improve activity across the series, however, significant enhancement was observed for selected derivatives. In particular, complex **7d′$_{Re}$** emerged as the most potent compound, exhibiting strong and selective activity against HuT-78, THP-1, and CCRF-CEM cells, while **9f′$_{Re}$** also demonstrated notable activity against leukemia cell lines. Mechanistic studies indicate that **8f′**, **9f′**, and **9g′** induce G1/G0 cell cycle arrest; **7g′**, **8f′**, and **9d′** decrease superoxide levels and disrupt mitochondrial membrane potential; and **7g′**, **8f′**, **9d′**, **9f′**, and **9g′** modulate the expression of key signaling proteins, including Akt, STAT3α, and STAT3β. In contrast, complex **7d′$_{Re}$** appears to exert its antiproliferative effects through a distinct mechanism, most likely involving modulation of the autophagic pathway in HuT-78 cells rather than activation of the classical apoptotic pathway.

Author contributions

Martina Piškor Benković: writing – original draft, formal analysis, investigation, methodology; Ivan Ćorić: investigation, formal analysis; Leon Sačer: investigation; Lorena Damjanović: investigation; Katarina Mišković Špoljarić: investigation, formal analysis; Berislav Perić: writing – original draft, formal analysis, methodology; Srećko I. Kirin: writing – original draft, review and editing; Ljubica Glavaš-Obrovac: writing – original draft, review and editing, supervision; Silvana Raić-Malić: writing – original draft, review and editing, supervision, project administration.

Conflicts of interest

There are no conflicts to declare.

Data availability

The data supporting this article have been included as part of the supplementary information (SI).

Supplementary information: ^{1}H NMR, ^{13}C NMR, FTIR, UV–vis spectra, and X-ray crystal structure. Ref. 79 and 80 are cited in the SI. See DOI: https://doi.org/10.1039/d6md00379f.

CCDC 2551645–2551647 contain the supplementary crystallographic data for this paper.[81a–c]

Acknowledgements

We greatly appreciate the financial support of the Croatian Science Foundation under the project HRZZ-IP-2022-10-9420.

References

1 N. Zhang, J. Wu, Q. Wang, Y. Liang, X. Li, G. Chen, L. Ma, X. Liu and F. Zhou, *Blood Cancer J.*, 2023, **13**, 82.
2 H.-S. Choi, B. S. Kim, S. Yoon, S.-O. Oh and D. Lee, *Int. J. Mol. Sci.*, 2024, **25**, 6639.
3 S. Valero-Diaz, C. Amato and B. Casar, *Kinases Phosphatases*, 2024, **2**, 255–267.
4 S. Devata and R. A. Wilcox, *Am. J. Clin. Dermatol.*, 2016, **17**, 225–237.
5 D. Ramesh, B. G. Vijayakumar and T. Kannan, *Eur. J. Med. Chem.*, 2020, **207**, 112801.
6 K. N. Venugopala and V. Kamat, *Pharmaceuticals*, 2024, **17**, 1258.
7 B. Nammalwar and R. A. Bunce, *Pharmaceuticals*, 2024, **17**, 104.
8 C. M. Marshall, J. G. Federice, C. N. Bell, P. B. Cox and J. T. Njardarson, *J. Med. Chem.*, 2024, **67**, 11622–11655.
9 G. Teli, R. Pal, L. Maji, G. S. Purawarga Matada and S. Sengupta, *J. Biomol. Struct. Dyn.*, 2024, **42**, 1582–1614.
10 S. Zuki, *Int. J. Mol. Sci.*, 2024, **25**, 9390.

11 T. Manna, S. Maji, M. Maity, B. Debnath, S. Panda, S. A. Khan, R. Nath and M. J. Akhtar, *Mol. Diversity*, 2024, **29**, 817–848.
12 L. Baziyar, P. Ahmadi, S. Zare Gheshlaghi, M. Behrouz, M. Emami, M. Saeedi, A. Ebrahimi, L. Emami and S. Khabnadideh, *J. Mol. Struct.*, 2024, **1302**, 137435.
13 P. Gugal, H. Kamurthy, R. Pal, G. S. P. Matada, M. Sanjay, C. M. Sowmya and P. M. Koushik, *Chem. Biodiversity*, 2026, **23**, e02639.
14 A. A. Al-Karmalawy, M. E. Eissa, T. A. Yousef, A. O. Al Khatib and S. S. Hawas, *RSC Adv.*, 2026, **16**, 3564–3579.
15 T. Gazivoda, S. Raić-Malić, V. Krištafor, D. Makuc, J. Plavec, S. Bratulić, S. Kraljević-Pavelić, K. Pavelić, L. Naesens, G. Andrei, R. Snoeck, J. Balzarini and M. Mintas, *Bioorg. Med. Chem.*, 2008, **16**, 5624–5634.
16 A. Meščić, A. Harej, M. Klobučar, D. Glavač, M. Cetina, S. K. Pavelić and S. Raić-Malić, *ACS Med. Chem. Lett.*, 2015, **6**, 1150–1155.
17 T. Gazivoda, M. Šokčević, M. Kralj, L. Šuman, K. Pavelić, E. De Clercq, G. Andrei, R. Snoeck, J. Balzarini, M. Mintas and S. Raić-Malić, *J. Med. Chem.*, 2007, **50**, 4105–4112.
18 A. M. Sajith, K. H. Narasimhamurthy, M. K. Shanmugam, S. Rangappa, S. Chandra Nayak, A. Chinnathambi, T. Awad Alahmadi, S. Ali Alharbi, K. R. Haridas, E. K. Reddy, B. Savitha, C. D. Mohan and K. S. Rangappa, *Bioorg. Med. Chem. Lett.*, 2021, **50**, 128332.
19 H. N. Dhara, B. Das, D. Barik, S. Manna and B. K. Patel, *Org. Lett.*, 2023, **25**, 9070–9075.
20 A. N. Volov, N. A. Volov and Y. B. Platonova, *Bioorg. Med. Chem. Lett.*, 2021, **48**, 128261.
21 A.-E. El Mansouri, A. Oubella, K. Dânoun, M. Ahmad, J. Neyts, D. Jochmans, R. Snoeck, G. Andrei, H. Morjani, M. Zahouily and H. B. Lazrek, *Arch. Pharm.*, 2021, **354**, e2100146.
22 C. Mcguigan, C. J. Yarnold, G. Jones, S. Velázquez, H. Barucki, A. Brancale, G. Andrei, R. Snoeck, E. De Clercq and J. Balzarini, *J. Med. Chem.*, 1999, **42**, 4479–4484.
23 P. S. Dhiwar, G. S. Purawarga Matada, R. Pal, E. Singh, A. Ghara, L. Maji, S. Sengupta and G. Andhale, *J. Biomol. Struct. Dyn.*, 2024, **42**, 1564–1581.
24 R. Kaczmarek, D. J. Twardy, T. L. Olson, D. Korczyński, G. Andrei, R. Snoeck, R. Dolot, K. A. Wheeler and R. Dembinski, *Eur. J. Med. Chem.*, 2021, **209**, 112884.
25 M. A. Aziz, R. A. T. Serya, D. S. Lasheen and K. A. M. Abouzid, *Futur. J. Pharm. Sci.*, 2016, **2**, 1–8.
26 M. M. A. Abd El-Mageed, A. A. M. Eissa, A. E. S. Farag and E. E. A. Osman, *Bioorg. Chem.*, 2021, **116**, 105336.
27 T. Wang, Y. Gao, F. Wu, L. Luo, J. Ma and Y. Hu, *RSC Med. Chem.*, 2024, **15**, 1565–1577.
28 H. Zhao, A. C. Donnelly, B. R. Kusuma, G. E. L. Brandt, D. Brown, R. A. Rajewski, G. Vielhauer, J. Holzbeierlein, M. S. Cohen and B. S. J. Blagg, *J. Med. Chem.*, 2011, **54**, 3839–3853.
29 M. A. Mansour, M. A. Oraby, Z. A. Muhammad, D. S. Lasheen, H. M. Gaber and K. A. M. Abouzid, *RSC Adv.*, 2022, **12**, 8193–8201.
30 S. Y. Lin, Y. Chang Hsu, Y. H. Peng, Y. Y. Ke, W. H. Lin, H. Y. Sun, H. Y. Shiao, F. M. Kuo, P. Y. Chen, T. W. Lien, C. H. Chen, C. Y. Chu, S. Y. Wang, K. C. Yeh, C. P. Chen, T. A. Hsu, S. Y. Wu, T. K. Yeh, C. T. Chen and H. P. Hsieh, *J. Med. Chem.*, 2019, **62**, 10108–10123.
31 M. C. Li, Y. L. Lai, P. H. Kuo, J. S. Reddy, C. M. Chen, J. Manimala, P. C. Wang, M. S. Wu, C. Y. Chang, C. M. Yang, C. Y. Lin, Y. C. Huang, C. H. Chiu, L. Chang, W. H. Lin, T. K. Yeh, W. C. Yen and H. P. Hsieh, *J. Med. Chem.*, 2024, **67**, 10906–10927.
32 R. K. V. Devambatla, O. A. Namjoshi, S. Choudhary, E. Hamel, C. V. Shaffer, C. C. Rohena, S. L. Mooberry and A. Gangjee, *J. Med. Chem.*, 2016, **59**, 5752–5765.
33 T. Gregorić, M. Sedić, P. Grbčić, A. Tomljenović Paravić, S. Kraljević Pavelić, M. Cetina, R. Vianello and S. Raić-Malić, *Eur. J. Med. Chem.*, 2017, **125**, 1247–1267.
34 L. Zhang, P. Liu, Y. Jiang, D. Fan, X. He, J. Zhang, B. Luo, J. Sui, Y. Luo, X. Fu and T. Yang, *Eur. J. Med. Chem.*, 2024, **272**, 116448.
35 G. N. Yatoo, B. A. Bhat, Z. U. K. Rather, M. Asif, S. A. Bhat, F. Gulzar, F. Rashied, A. H. Wani, I. Ahmed, S. M. Zargar, M. A. Mir and J. A. Banday, *Fitoterapia*, 2024, **175**, 105927.
36 P. S. Zinman, A. Welsh, R. O. Omondi, S. Khan, S. Prince, E. Nordlander and G. S. Smith, *Eur. J. Med. Chem.*, 2024, **266**, 116094.
37 M. O. Dar, R. H. Mir, R. Mohiuddin, M. H. Masoodi and F. A. Sofi, *J. Inorg. Biochem.*, 2023, **246**, 112290.
38 N. Montesdeoca, R. L. Borkar, M. Sathiyendiran and J. Karges, *Chem. – A Eur. J.*, 2024, **30**, 1–6.
39 T. S. de Lavor, M. H. S. Teixeira, P. A. de Matos, R. C. Lino, C. M. F. Silva, M. E. G. do Carmo, M. E. Beletti, A. O. T. Patrocinio, R. J. de Oliveira Júnior and T. M. Tsubone, *J. Inorg. Biochem.*, 2024, **257**, 112600.
40 S. Jakopec, L. Gourdon-Grünewaldt, I. Čipor, A. Meščić Macan, B. Perić, I. Piantanida, K. Cariou, G. Gasser, S. I. Kirin and S. Raić-Malić, *Dalton Trans.*, 2023, **52**, 9482–9498.
41 M. Piškor, I. Ćorić, B. Perić, K. M. Špoljarić, S. I. Kirin, L. Glavaš-Obrovac and S. Raić-Malić, *J. Inorg. Biochem.*, 2025, **262**, 112770.
42 M. Piškor, M. Ter, L. Persoons, D. Daelemans, A. Adel, M. O. Taha, A. Milić, M. Sedić and S. Raić-Malić, *RSC Adv.*, 2025, **15**, 50633–50651.
43 S. Djaković, L. Glavaš-Obrovac, J. Lapić, S. Maračić, J. Kirchofer, M. Knežević, M. Jukić and S. Raić-Malić, *Appl. Organomet. Chem.*, 2021, **35**, 1–16.
44 A. B. Solea, G. Demirci, F. M. Harvey, A. Crochet, F. Zobi and O. Mamula Steiner, *Dalton Trans.*, 2024, **53**, 13743–13755.
45 S. Le Garrec, D. Martins-Bessa, M. Wolff, B. Delavaux-Nicot, S. Mallet-Ladeira, C.-L. Serpentini, E. Benoist, F. Bedos-Belval and S. Fery-Forgues, *Dalton Trans.*, 2024, **53**, 16512–16529.
46 C. C. Konkankit, B. A. Vaughn, S. N. MacMillan, E. Boros and J. J. Wilson, *Inorg. Chem.*, 2019, **58**, 3895–3909.
47 H. C. Bertrand, S. Clède, R. Guillot, F. Lambert and C. Policar, *Inorg. Chem.*, 2014, **53**, 6204–6223.
48 L. E. Enslin, K. Purkait, M. D. Pozza, B. Saubamea, P. Mesdom, H. G. Visser, G. Gasser and M. Schutte-Smith, *Inorg. Chem.*, 2023, **62**, 12237–12251.

 This journal is © The Royal Society of Chemistry 2026

49 A. Marco, P. Ashoo, S. Hernández-García, P. Martínez-Rodríguez, N. Cutillas, A. Vollrath, D. Jordan, C. Janiak, F. Gandía-Herrero and J. Ruiz, *J. Med. Chem.*, 2024, **67**, 7891–7910.
50 B. L. Murphy, S. C. Marker, V. J. Lambert, J. J. Woods, S. N. MacMillan and J. J. Wilson, *J. Organomet. Chem.*, 2020, **907**, 121064.
51 M. Piškor Benković, L. Sačer, R. Abhirami, S. K. Singh, M. Sedić, L. Persoons, D. Daelemans, B. Perić, S. I. Kirin and S. Raić-Malić, *J. Mol. Struct.*, 2026, **1366**, 146076.
52 R. Foy, L. Crozier, A. U. Pareri, J. M. Valverde, B. H. Park, T. Ly and A. T. Saurin, *Mol. Cell*, 2023, **83**, 4047–4061.e6.
53 A. Mahapatra, T. Prasad and T. Sharma, *Future J. Pharm. Sci.*, 2021, **7**, 123.
54 J. Liu, Y. Peng and W. Wei, *Trends Cell Biol.*, 2022, **32**, 30–44.
55 M. Moradi, A. Mousavi, E. Řezníčková, F. Peytam, M. Peřina, V. Vojáčková, L. Firoozpour, R. Jorda, J. Grúz, Z. Emamgholipour, S. E. Sadat-Ebrahimi, V. Kryštof and A. Foroumadi, *Eur. J. Med. Chem.*, 2024, **280**, 116962.
56 P. Carpintero-Fernández, M. M. Martínez, A. Carneiro-Figueira, R. Martínez, A. García-Yuste, M. Barturen-Gómez, C. Pérez-Caaveiro, A. Guitián-Caamaño, L. A. Sarandeses, J. P. Sestelo and M. D. Mayán, *Mol. Ther. Oncol.*, 2026, **34**, 201129.
57 K. Takács-Vellai, *Int. J. Mol. Sci.*, 2023, **24**, 11609.
58 J. Debnath, N. Gammoh and K. M. Ryan, *Nat. Rev. Mol. Cell Biol.*, 2023, **24**, 560–575.
59 K. Schindler and F. Zobi, *Molecules*, 2022, **27**, 539.
60 B. Perillo, M. Di Donato, A. Pezone, E. Di Zazzo, P. Giovannelli, G. Galasso, G. Castoria and A. Migliaccio, *Exp. Mol. Med.*, 2020, **52**, 192–203.
61 Y. Zhang, Y. Wang, Y. Zhao, W. Gu, Y. Zhu and S. Wang, *RSC Adv.*, 2019, **9**, 29711–29720.
62 L. D. Zorova, V. A. Popkov, E. Y. Plotnikov, D. N. Silachev, I. B. Pevzner, S. S. Jankauskas, V. A. Babenko, S. D. Zorov, A. V. Balakireva, M. Juhaszova, S. J. Sollott and D. B. Zorov, *Anal. Biochem.*, 2018, **552**, 50–59.
63 C. M. Gorospe, G. Carvalho, A. H. Curbelo, L. Marchhart, I. C. Mendes, K. Niedźwiecka and P. H. Wanrooij, *Life Sci. Alliance*, 2023, **6**, 1–14.
64 K. Berkley, J. Zalejski and A. Sharma, *Cancers*, 2025, **17**, 755.
65 A. Kashyap, J. Dai and X. Ni, *Cancers*, 2025, **17**, 568.
66 P. A. H. Ehm and C. Rehbach, *Lymphatics*, 2025, **3**, 33.
67 S. Sikka, R. Surana, X. Dai, J. Zhang, A. P. Kumar, B. K. H. Tan, G. Sethi and A. Bishayee, *Biochim. Biophys. Acta - Rev. Cancer*, 2014, **1845**, 136–154.
68 Z.-Y. Zheng, P.-L. Yang, W. Luo, S.-X. Yu, H.-Y. Xu, Y. Huang, R.-Y. Li, Y. Chen, X.-E. Xu, L.-D. Liao, S.-H. Wang, H.-C. Huang, E.-M. Li and L.-Y. Xu, *Cancers*, 2021, **13**, 901.
69 M. Mustafa, R. Ahmad, I. Q. Tantry, W. Ahmad, S. Siddiqui, M. Alam, K. Abbas, Moinuddin, M. I. Hassan, S. Habib and S. Islam, *Cell*, 2024, **13**, 1838.
70 W. A. El-Sayed and A. A.-H. Abdel-Rahman, *Z. Naturforsch. B*, 2010, **65**, 57–66.
71 S. Liu, W. Wei, Y. Li, X. Liu, X. Cao, K. Lei and M. Zhou, *Eur. J. Med. Chem.*, 2015, **95**, 473–482.
72 X. Z. Wang, J. Jia, Y. Zhang, W. R. Xu, W. Liu, F. N. Shi and J. W. Wang, *J. Chin. Chem. Soc.*, 2007, **54**, 643–652.
73 M. R. Boyd and K. D. Paull, *Drug Dev. Res.*, 1995, **34**, 91–109.
74 T. Mosmann, *J. Immunol. Methods*, 1983, **65**, 55–63.
75 J. Schindelin, I. Arganda-Carreras, E. Frise, V. Kaynig, M. Longair, T. Pietzsch, S. Preibisch, C. Rueden, S. Saalfeld, B. Schmid, J.-Y. Tinevez, D. J. White, V. Hartenstein, K. Eliceiri, P. Tomancak and A. Cardona, *Nat. Methods*, 2012, **9**, 676–682.
76 *Rigaku Oxford Diffraction CrysAlisPro*, Oxford, UK, 2018.
77 G. M. Sheldrick, *Acta Crystallogr., Sect. A: Found. Adv.*, 2015, **71**, 3–8.
78 G. M. Sheldrick, *Acta Crystallogr., Sect. C: Struct. Chem.*, 2015, **71**, 3–8.
79 L. J. Farrugia, *J. Appl. Crystallogr.*, 2012, **45**, 849–854.
80 C. F. Macrae, P. R. Edgington, P. McCabe, E. Pidcock, G. P. Shields, R. Taylor, M. Towler and J. Van De Streek, *J. Appl. Crystallogr.*, 2006, **39**, 453–457.
81 (*a*) CCDC 2551645: Experimental Crystal Structure Determination, 2026, DOI: 10.5517/ccdc.csd.cc2rn64s; (*b*) CCDC 2551646: Experimental Crystal Structure Determination, 2026, DOI: 10.5517/ccdc.csd.cc2rn65t; (*c*) CCDC 2551647: Experimental Crystal Structure Determination, 2026, DOI: 10.5517/ccdc.csd.cc2rn66v.